perfusion was carried out at 1.0 μl/min with artificial striatal cerebrospinal fluid (aCSF: Na^+, 155.0 mM; Ca^{2+}, 1.1 mM; K^+, 2.9 mM; Mg^{2+}, 0.8 mM; and Cl^-, 155.6 mM; pH 7.4). After a 4-h equilibration period, the perfusates were collected every 30 min. The basal level of DA was determined by averaging the DA levels of eight dialysates collected during a 4-h period. The DA level due to Ca^{2+}-dependent efflux was the difference between the basal level and the average level in two consecutive dialysates collected within 1 h after perfusion of Ca^{2+}-free aCSF for 2 h. Samples were assayed for DA or DOPAC using HPLC-EC.

2.8. Electrophysiology

The midbrain slices and corticostriatal slices prepared from 3–4-week-old mice were cut coronally and parasagittally, respectively (250 μm thick), transferred to an incubation chamber and allowed to recover for 1 h before recording. During recording, a slice was perfused continuously with aCSF (124 mM NaCl, 3 mM KCl, 1 mM NaH_2PO_4, 1.2 mM $MgCl_2$, 2.4 mM $CaCl_2$, 10 mM glucose, 26 mM $NaHCO_3$, pH 7.4) saturated with 95% O_2, and 5% CO_2 at a rate of 1–2 ml/min at 30 °C. Whole-cell patch-clamp recordings were made from DA neurons in midbrain slices or striatal medium spiny neurons (MSNs) in corticostriatal slices by an EPC9/2 amplifier (HEKA Elektronik Lambrecht/Pfalz, Germany) with infrared differential contrast visualization using an Olympus BX50WI (Tokyo, Japan) and a CCD camera. For current-clamp recordings, patch pipettes contained 129 mM K-gluconate, 11 mM KCl, 2 mM $MgCl_2$, 10 mM HEPES, 4 mM Na_2-ATP, 0.3 mM GTP, and 0.5% biocytin (brought to pH 7.3 with KOH; osmolarity 280 mOsm). Hyperpolarizing and depolarizing current injection was made to study the physiological properties of DA neurons. For voltage-clamp recordings, patch pipettes (4–6 MΩ) were filled with 124 mM Cs-methanesulfonate, 11 mM KCl, 2 mM $MgCl_2$, 10 mM HEPES, 4 mM Na_2-ATP, 0.3 mM GTP, 0.1 mM spermine, 5 mM QX-314, and 0.5% biocytin and brought to 280 mOsm and pH 7.3 with CsOH. Inhibitory postsynaptic currents (IPSCs) were evoked by electrical stimulation of the striatum with a bipolar tungsten electrode in the presence of the *N*-methyl-D-aspartate receptor antagonist *D*(−)-2-amino-5-phosphonopentanoic acid (D-AP5, 25 μM) and the α-amino-3-hydroxy-5-methyl-4-isoxazolepropionic acid receptor antagonist 6-cyano-7-nitroquinoxaline-2,3-dione (CNQX, 20 μM). Effects of paired pulse stimulation were then investigated by delivering five pairs of stimuli at decreasing intervals (500, 200, 100, 50, and 25 ms). Thirty stimulus pulses given 70 ms apart (about 14 Hz) were next applied three times every 20 s. Nomifensine (3 μM), an uptake inhibitor of DA, was then bath-applied. Voltage errors attributable to the liquid junction potential (11 mV) were subtracted. Signals were filtered at 5 kHz and digitized at 20 kHz with Pulse/PulseFit (HEKA). If series resistance was changed by >20%, the experiments were discarded. To confirm the morphology of the recorded neurons, the slices containing biocytin-filled cells were fixed and stained with Vectastain ABC kit (Vector Laboratories). Areas of cell bodies of DA neurons were measured using NIH Image J software (http://rsb.info.nih.gov/ij/). Statistical significance was assessed by unpaired or paired Student's *t*-tests. D-AP5 was obtained from Tocris Cookson and all other drugs from Sigma.

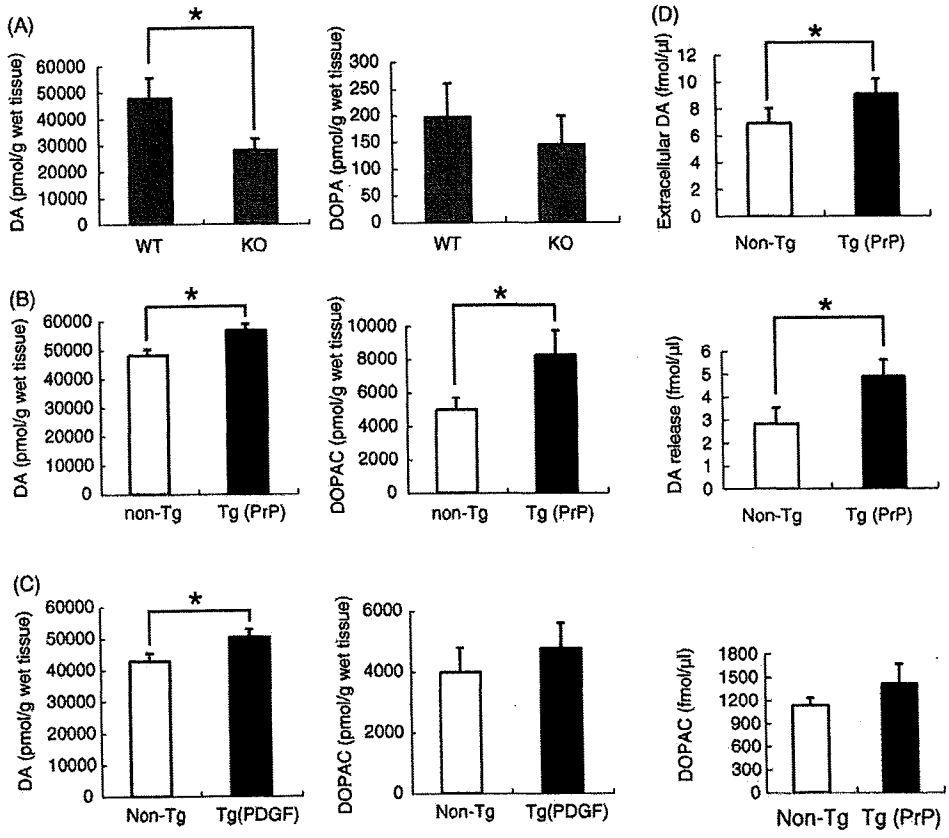

Fig. 2. DA and its metabolites in the striatum of Pael-R Tg and Pael-R KO mice. (A) Striatal tissue levels of DA (left) and L-DOPA (right) in Pael-R KO and WT littermate mice measured by HPLC-EC ($n = 6$ each). Results are presented as the mean ± S.E.M. for six animals at 13-months of age. *$P < 0.05$ *vs.* WT by Student's *t*-test. (B) Striatal tissue levels of DA and DOPAC in PrP-Tg and non-Tg littermate mice measured by HPLC-EC. Results are presented as the mean ± S.E.M. for 15 animals at 10-months of age. *$P < 0.05$ *vs.* non-Tg by Student's *t*-test. (C) Striatal tissue levels of DA and DOPAC in PDGFβ-Tg and non-Tg littermate mice measured by HPLC-EC. Results are presented as the mean ± S.E.M. for 12 animals at 15 months of age. *$P < 0.05$ *vs.* non-Tg by Student's *t*-test. (D) Extracellular DA levels (upper), DOPAC levels (lower), and Ca^{2+}-dependent DA release (middle) in the striatum of free moving PrP-Tg and non-Tg littermate mice at 10 months of age measured by microdialysis (mean ± S.E.M., $n = 10$ each). *$P < 0.05$ *vs.* non-Tg by Student's *t*-test.

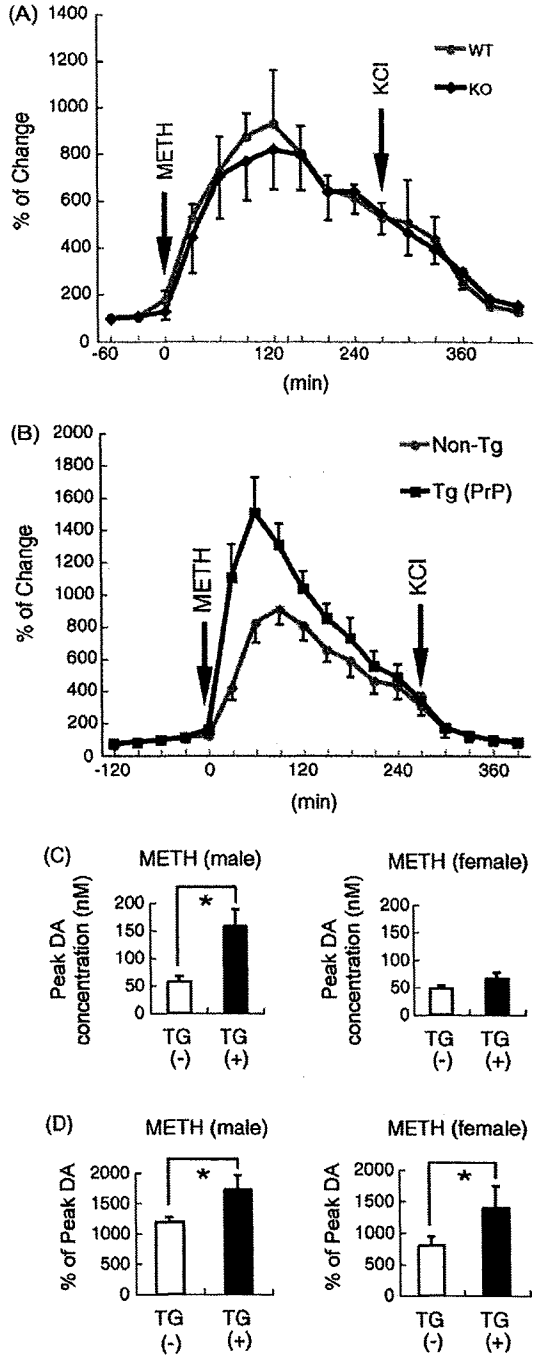

Fig. 3. Hypersensitivity to methamphetamine in Pael-R Tg mice. (A) Time course of DA release in the striatum of Pael-R KO ($n = 8$) and WT littermate mice ($n = 8$) in response to methamphetamine (METH, 30 mg/kg, s.c.). Perfusion of medium containing 100 mM KCl through the microdialysis probe at 270 min after METH stimulation did not show another peak of DA release, suggesting that almost all of the intracellular DA was released by this METH administration. The values are represented as the mean ± S.E.M. of percentage to basal levels (average of the levels at 30 and 60 min before METH administration) for eight animals at 6–12 months of age. (B) Time course of DA release in the striatum of PrP-Tg ($n = 10$) and non-Tg littermate mice ($n = 10$) in response to METH (30 mg/kg, s.c.) and subsequent KCl (100 mM) administration as in (A). The values for 10 animals at 6 months of age are represented as in (A). DA release after METH stimulation in PrP-Tg was significantly different by repeated measures ANOVA [genotype × time interaction, $F(1,245) = 27.1$; $P < 0.001$]. (C) The peak values of striatal DA efflux after METH treatment in PrP-Tg male (left, $n = 5$ each group) and female (right, $n = 5$ each group) mice are shown. *$P < 0.05$ *vs.* non-Tg by Student's *t*-test. (D) Percent of the peak DA efflux to basal DA content after METH treatment in PrP-Tg male (left, $n = 5$ each group) and female (right, $n = 5$ each group) mice is shown. *$P < 0.05$ *vs.* non-Tg by Student's *t*-test.

3. Results

3.1. Generation of Pael-R Tg and Pael-R KO mice

Tg mice were generated expressing human Pael-R under the control of the PrP promoter and the PDGF β2 promoter (Fig. 1A). Several lines of Tg mice were obtained, and mice with the highest expression levels of Pael-R were chosen from each promoter group and characterized (Fig. 1B). The PrP promoter-driven transgenic (PrP-Tg) line PrP1 (maintained on a mixed genetic background of C3H × B6), showed high expression of Pael-R transgene in the whole brain, while the PDGF β2 promoter-driven transgenic (PDGFβ-Tg) line 20 on a B6 background showed marked expression in the striatum and the midbrain compared with other regions (Fig. 1B). The expression of Pael-R transgene in TH-positive neurons in the SN was immunohistochemically confirmed by increased Pael-R immunosignals compared with that of non-Tg mice (data not shown).

Murine Pael-R gene contains two exons (Marazziti et al., 1998). The first exon containing a start codon was targeted to generate Pael-R-deficient mice on a B6 background. Two loxP sites flanking exon 1 and a selection marker cassette were introduced into the mouse Pael-R gene by means of homologous recombination in ES cells (Fig. 1C, targeted allele). To generate a null allele, part of the exon 1 and the selection marker were removed by *in vitro* fertilization using sperm from a heterozygote mouse bearing the targeted allele and subsequent microinjection of Cre recombinase cDNA into the fertilized eggs. Homologous recombination of the targeting construct and the deletion of the floxed cassette were confirmed by Southern blotting (data not shown). To determine the level of expression of Pael-R transcripts, Northern blotting analysis was performed with total RNA from whole brain samples (Fig. 1D). This analysis indicated that in mice carrying both the targeted and null alleles, the expression of Pael-R mRNA transcripts is completely lost, suggesting that the insertion of loxP or the selection cassette on non-coding regions has disrupted a critical element(s) for transcripton.

The protein levels of expression in Pael-R Tg and KO mice were assessed by Western blotting with membrane fractions prepared from whole brain of samples with anti-Pael-R Ab (Fig. 1E). PrP-Tg and PDGFβ-Tg mice had respectively ~12 and ~5.5 times higher Pael-R protein levels compared with normal mice (+/+), while homozygote mice bearing the null allele or targeted allele failed to show an immunosignal of the Pael-R protein (Fig. 1E and F) The alterations of Pael-R expression had no effect on the expression of LP-2, whose gene has the highest homology with the Pael-R gene (Fig. 1E) (Valdenaire et al., 1998).

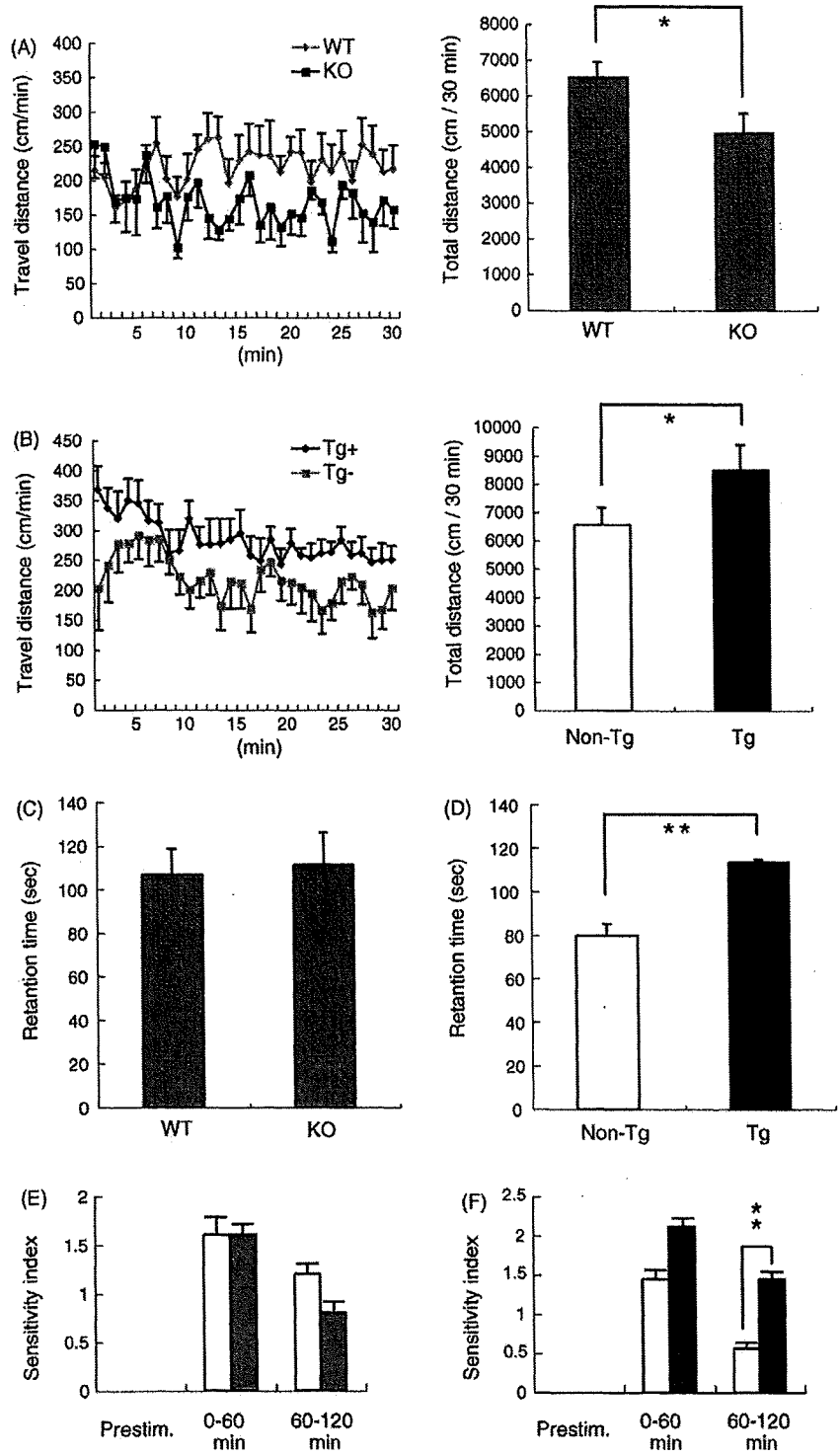

Fig. 4. Locomotor activity of Pael-R Tg and Pael-R KO mice. (A) Spontaneous horizontal migration of Pael-R KO ($n = 9$) and WT littermate ($n = 11$) mice at 1 year of age over a period of 30 min just after introduction into the open field chamber (50 cm × 50 cm). The migration distance in each minute interval after introduction (left) and total migration distance (right) are represented as mean ± S.E.M. (*$P < 0.05$ *vs.* WT; Student's *t*-test). (B) Spontaneous horizontal migration of PrP-Tg ($n = 11$) and non-Tg littermate ($n = 9$) mice at 1 year of age over a period of 30 min as in A. *$P < 0.05$ *vs.* non-Tg by Student's *t*-test. (C) Motor coordination of Pael-R KO and WT littermate mice at 1 year of age was assessed with the rotarod test ($n = 10$ each group). The retention time on a rotating wheel was consecutively measured four times. Each trial lasted for a maximum of 5 min, during which time the wheel rotates with a linear acceleration from 4 to 40 rpm. Data are represented as mean ± S.E.M. of retention time. (D) Motor coordination of PrP-Tg and non-Tg mice at 1 year of age was assessed with the rotarod test as in (C). (**$P < 0.01$ *vs.* non-Tg; Student's *t*-test, $n = 10$ each group). (E) The behavior of Pael-R KO and WT littermate male mice ($n = 5$ each group) during the free moving *in vivo* microdialysis analysis before and after METH administration (30 mg/kg) in Fig. 3A was scored as follows: 0, none; 1, piloerection without rotational motion; 2, slow rotational motion; 3, fast rotational motion or jumping movement. Mean ± S.E.M. of the score are represented as Sensitivity Index. Grey bars, KO mice; white bars, WT

3.2. Abnormal DA synthesis and metabolism by altered Pael-R expression

Pael-R Tg and KO mice are viable and present no gross anatomical abnormalities. Pael-R KO mice gained weight normally, whereas Pael-R Tg mice gained at a slower rate (37.1 ± 4.1 g in PrP-Tg *versus* 47.1 ± 2.1 g in PrP-non-Tg males at 10 months, $P < 0.05$, $n = 7$; 30.6 ± 1.9 g in PrP-Tg *versus* 38.5 ± 2.4 g in PrP-non-Tg females at 10 months, $P < 0.01$, $n = 14$; and 23.0 ± 1.7 g in PDGFβ-Tg *versus* 30.2 ± 1.8 g in PDGFβ-non-Tg males at 6 months, $P < 0.05$, $n = 9$).

Because Pael-R is abundantly expressed in the DA neurons and is implicated in the pathogenesis of PD, we then examined the effect of altered Pael-R expression on the nigrostriatal pathway. In the whole striatum tissue of Pael-R KO mice, DA, but not its precursor L-DOPA, levels were reduced to 60% of that in wild-type (WT) littermates (Fig. 2A). In contrast, striatal levels of DA were increased in both strains of Pael-R Tg mice (Fig. 2B and C). The levels of DOPAC were significantly increased only in PrP-Tg mice (Fig. 2B and C). In PrP-Tg mice, the concentration of extracellular DA (measured by *in vivo* microdialysis of freely moving mice) in the striatum as well as the concentration due to Ca^{2+}-dependent release at the presynapse of DA neurons was increased (Fig. 2D). The concentrations of extracellular DA and DOPAC (measured by *in vitro* microdialysis) were not significantly different in the striatum of Pael-R KO mice (data not shown).

3.3. Increased DA storage and release in Pael-R Tg mice

Administration of the psychostimulant methamphetamine (METH) stimulates DA release from the presynapse of DA neurons. METH administration (30 mg/kg, s.c.) induced a similar increase in extracellular DA levels in Pael-R KO and WT littermate mice (Fig. 3A). No increase occurred when 100 mM KCl was infused intrastriatally *via* a microdialysis probe at 270 min after METH, suggesting that 30 mg/kg METH is sufficient to the release of almost all DA stored in the presynapse. By contrast, METH administration (30 mg/kg, s.c.) stimulates a significant increase (~1.6-fold) in extracellular DA level in PrP-Tg compared with non-Tg mice ($P < 0.001$ by repeated measures ANOVA; Fig. 3B). Following METH administration, dialysate levels of DOPAC were decreased similarly in both PrP-Tg and PrP-non-Tg mice as well as Pael-R KO mice (data not shown), suggesting that METH inhibits monoamine oxidase activity as previously reported (Fumagalli et al., 1998). Although actual value of DA efflux was larger in male mice than in female mice, there was no sex difference in the ratio of peak DA levels to basal DA levels (Fig. 3C and D).

3.4. Behavioral phenotype by mice with altered Pael-R expression

DA content in the striatum plays an important role in the control of locomotor and stereotypic behavior. Changes in DA levels in these mice led us to test locomotor activity. The spontaneous locomotor activity of naïve Pael-R KO mice was significantly reduced in an initial 30-min trial (Fig. 4A). However, whereas the locomotor activity of Pael-R KO mice did not change every month, that of WT littermates gradually declined, probably because of habituation to the test. Consequently, locomotor activity was higher in Pael-R KO mice than WT littermates 5 months later (data not shown). The result suggests that Pael-R KO mice somewhat lose the ability of habituation to a circumstance. In contrast to Pael-R KO mice, both PrP-Tg and PDGFβ-Tg mice showed elevated locomotor activity in the same test (Fig. 4B and data not shown).

Motor performance was assessed by the rotarod test as described previously (Tateno et al., 2004). The rotarod scores measured of 6-month-old and 1-year-old Pael-R KO mice were not significantly changed whereas 1-year-old PrP-Tg showed the significant improvement in this test (Fig. 4C and D and data not shown). The phenotypes of Pael-R Tg mice in the locomotor test and the rotarod test might be suggested to reflect an elevated extracellular DA content.

Behavior in response to the METH-treatment (30 mg/kg, s.c.) was assessed in Pael-R KO mice and PrP-Tg mice (Fig. 4E and F). The responses to METH of Pael-R KO male mice did not significantly differ from that of their WT male littermates (Fig. 4E). However, these responses were more sensitive in PrP-Tg mice than in non-Tg littermates (Fig. 4F). These results correlated well with the DA release data obtained in the *in vivo* microdialysis experiment (Fig. 3A and B). The female responses tended to be milder than male, although levels of Pael-R protein expression in the brain were not different between male and female PrP-Tg mice (data not shown).

3.5. Sensitivity to DA neurotoxins

The numbers of TH-immunoreactive neurons in the SN, the ventral tegmental area (VTA) and the locus coeruleus of Pael-R KO and PrP-Tg mice (which are highly expressed in the locus coeruleus as well as the SN and VTA unlike PDGFβ-Tg mice) showed age-dependent loss of TH-positive neurons (manuscript in submission). The number of TH neurons in Pael-R KO mice showed a slight reduction compared with their WT littermates (Fig. 5A). However, the number did not change over time, suggesting that Pael-R somewhat contribute to developmental regulation of TH-positive neurons (data not shown).

Parkin KO mice have an increased extracellular DA and whole striatal DOPAC levels (Goldberg et al., 2003; Itier et al., 2003). Both Parkin KO mice and Pael-R Tg mice appear to have

littermates; Prestim., before METH-treatment; 0–60 min, for the first 1 h of METH-treatment; 60–120 min, for the second 1 h. (F) The behavior of PrP-Tg and non-Tg mice ($n = 5$ males; $n = 4$ females in each genotype) in METH administration (30 mg/kg) was scored as in (D). The score representing the sensitivity to METH is higher in the second 1 h after METH administration compared with non-Tg littermate (**$P < 0.01$ by Mann–Whitney U-test). Black bars, Tg mice; and white bars, non-Tg littermates.

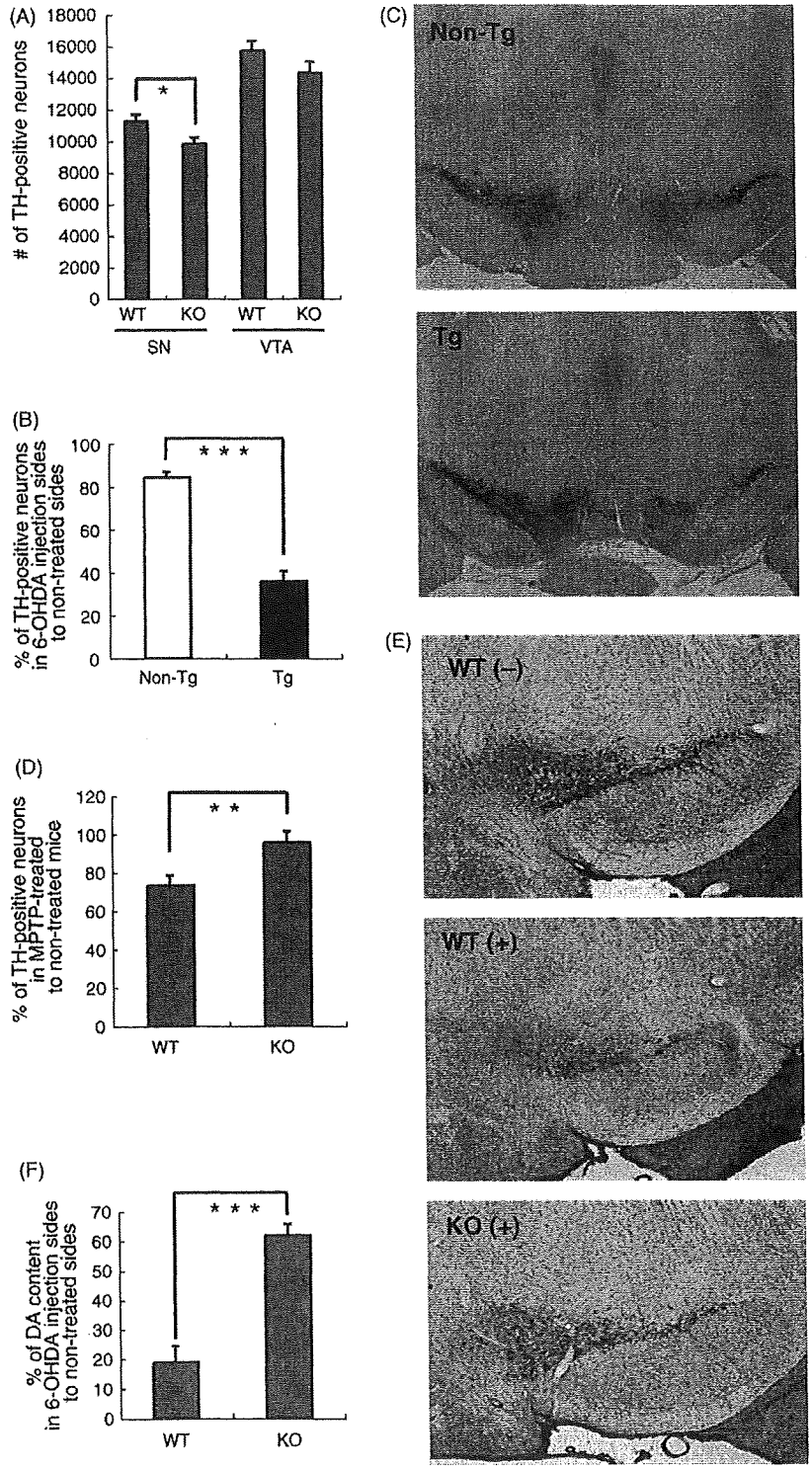

Fig. 5. Sensitivity of DA neurons to the neurotoxins in Pael-R Tg and Pael-R KO mice. (A) The estimated number of TH-positive neurons in the SN and VTA of Pael-R KO and WT littermate mice at 3 months of age was assessed by a stereological method (mean ± S.E.M., $n = 7$ mice). *$P < 0.05$ *vs.* WT littermates by Student's *t*-test. (B) Effect of 6-OHDA on DA neurons of Pael-R Tg mice 21 days after administration. 6-OHDA was injected into the left striatum of PrP-Tg and non-Tg littermate mice at 2–3 months of age. The number of TH-immunopositive neurons in the SN was assessed by a stereological method. To correct for genotype-based differences in the number of TH-positive cells, data are represented as percentage of the number on the non-treated side (right striatum) of each animal (mean ± S.E.M., Tg, $n = 8$; non-Tg, $n = 9$). ***$P < 0.001$ *vs.* non-Tg by Student's *t*-test. (C) Representative coronal sections of 6-OHDA-treated non-Tg (upper) and Tg (lower) brains containing the SN are shown. The 6-OHDA-treated SN is located on the left side. (D) Effect of MPTP on DA neurons of Pael-R KO mice 7 days after administration. MPTP was injected into Pael-R KO and WT littermate mice at 3 months of age. Data are represented as percentage of the number of DA neurons in the SN in each pair with saline treatment (mean ± S.E.M., $n = 8$ per each group). **$P < 0.01$ *vs.* non-Tg by Student's *t*-test. (E) Representative coronal sections of

this phenotype. Although DA neurons in the SN of Parkin KO mice do not show axonal degeneration or neuronal death with age like those of AR-JP patients, there is some evidence that DA neurons in Parkin KO mice are functionally disturbed. Therefore, we expected that DA neurons in Pael-R Tg mice might be subjected to stress to deal with elevated DA content. DA neurotoxins 6-OHDA and MPTP, which have been used to develop PD animal models, behave as catecholaminergic or DA neuron-specific neurotoxins (Betarbet et al., 2002). To evaluate the vulnerability of mice with altered Pael-R expression to these neurotoxins, the number of TH-immunopositive neurons in the SN or the amounts of DA in the striatum was evaluated after the treatment. The SN of PrP-Tg and non-Tg littermates that were treated with 6-OHDA-injection into the left striatum showed, respectively, 64% and 16% reduction of TH-immunopositive neurons compared with the untreated hemisphere (Fig. 5B and C). In contrast, MPTP-treatments of WT and Pael-R KO mice led to 27% and 4% fewer TH-immunoreactive neurons, respectively, than counted in saline-treated WT mice (Fig. 5D and E). The amount of striatal DA in Pael-R KO mice and WT littermates 3 weeks after 6-OHDA-injection into the left striatum showed, respectively, 38% and 81% reduction compared with the untreated hemisphere (Fig. 5F). These results indicate that DA neurons in PrP-Tg mice are more sensitive to DA neurotoxins, suggesting that these DA neurons are potentially stressed. Conversely, DA neurons in Pael-R KO mice appeared to be less sensitive (i.e., to have the opposite characteristics from that in PrP-Tg mice).

3.6. Electrophysiological analysis of DA neurons in Pael-R-KO and PrP-Tg mice

To study how the function of DA neurons was influenced by the expression of Pael-R, we made the whole-cell patch-clamp recordings from DA neurons in midbrain slices and slices containing the striatum prepared from Pael-R KO and PrP-Tg mice of postnatal 3–4 weeks. In both DA neurons of Pael-R KO (WT, $n = 36$ cells, KO, $n = 39$ cells) and PrP-Tg (non-Tg, $n = 28$ cells, Tg, $n = 28$ cells) mice we found no changes in the resting membrane potentials (WT, -55.4 ± 0.8 mV, KO, -55.0 ± 0.7 mV; non-Tg, -57.2 ± 0.9 mV, Tg, -55.3 ± 1.2 mV), the spike thresholds (WT, -30.0 ± 0.5 mV, KO, -29.8 ± 0.6 mV; non-Tg, -29.5 ± 0.5 mV, Tg, -30.4 ± 0.4 mV), the peak values (WT, 26.9 ± 1.1 mV, KO, 26.8 ± 1.1 mV; non-Tg, 27.8 ± 1.3 mV, Tg, 27.3 ± 1.3 mV), and amplitudes (WT, 56.9 ± 1.0 mV, KO, 56.6 ± 1.3 mV; non-Tg, 57.4 ± 1.2 mV, Tg, 57.6 ± 1.3 mV) of action potentials, the spike widths at half amplitude (WT, 1.46 ± 0.05 ms, KO, 1.47 ± 0.06 ms; non-Tg, 1.57 ± 0.06 ms, Tg, 1.53 ± 0.06 ms), spontaneous firing frequencies (WT, 2.87 ± 0.20 Hz, KO, 2.50 ± 0.20 Hz; non-Tg, 1.85 ± 0.13 Hz, Tg, 1.81 ± 0.15 Hz), and firing patterns. However, the input resistance of DA neurons of PrP-Tg mice was slightly larger (Student's t-test, $P < 0.05$; Fig. 6A) than that of the non-Tg control neurons although there was no difference between DA neurons of Pael-R KO and WT mice (data not shown). Interestingly, the input resistance in the striatal MSNs was smaller in Pael-R KO mice (WT, $n = 16$, 133.3 ± 18.9 MΩ; KO, $n = 14$, 57.6 ± 9.8 MΩ, $P < 0.01$) and larger in PrP-Tg mice (non-Tg, $n = 19$, 81.9 ± 22.3 MΩ; Tg, $n = 22$, 146.2 ± 21.4 MΩ, $P < 0.05$) than their respective controls (data not shown). Since the factors which determine the input resistance are the cell size and the density and permeability of various types of ion channels incorporated into the cell membrane, our finding that the cell size of the Tg DA neurons was similar to that of non-Tg controls (soma area: non-Tg, 303 ± 14 μm^2, $n = 29$; Tg, 286 ± 16 μm^2, $n = 26$; $P > 0.4338$) suggests a possible interaction of Pael-R with a certain membranous component.

Electrical stimulation of cortico- and nigro-striatal pathways in striatal slices evokes release of DA from the residual dopaminergic nerve terminals (Calabresi et al., 1995). The released DA then depresses GABAergic IPSC in the striatal MSNs by activation of presynaptic DA D2 receptors (Bamford et al., 2004; Centonze et al., 2002, 2003, 2004). We thus performed paired pulse stimulation to get paired pulse ratios (PPRs) of the second IPSC amplitudes to the first in the MSN to study a change in DA release in Pael-R KO and PrP-Tg mice. We found no statistical change in PPRs in both Pael-R KO and PrP-Tg mice with respect to their respective controls (upper left in Fig. 6B, and data not shown). Nomifensine is a selective DA uptake inhibitor interacting with the DA transporter at a site different from that of cocaine. A previous report demonstrated that both cocaine and amphetamine, more potent drugs than nomifensine, increased the DA content and suppressed IPSCs through activation of presynaptic DA D2 receptors (Centonze et al., 2002; Wieczorek and Kruk, 1994). After nomifensine application there was a slight increase in PPR in WT and a decrease in KO at an interval of 100 ms, yielding a significant difference only in Pael-R KO mice (lower left in Fig. 6B, $P < 0.05$). Furthermore, we found a significant decrease in IPSC amplitudes upon repeated low frequency stimulation (30 pulses applied 70 ms apart) both before and after application of nomifensine in Pael-R KO mice (right in Fig. 6B). In contrast, no change was observed in PPRs and IPSC amplitudes with paired pulse stimulation and repeated low frequency stimulation before and after nomifensine in PrP-Tg mice (data not shown). In both types of mice there were no changes in rise time and decay time constant of IPSC, suggesting no alterations in $GABA_A$ receptor channel kinetics *per se* (data not shown).

These results suggest that in Pael-R KO mice DA is significantly less released while electrophysiological properties of DA neurons remain unchanged. On the other hand, we did not observe any significant changes in DA neurons of PrP-Tg mice except for a small increase in input resistance probably because

MPTP-treated (+) or saline-treated (−) brains containing the SN are shown. (F) Effect of 6-OHDA on DA neurons of Pael-R KO mice. 6-OHDA was injected as in B at 2–3 months of age. The amount of DA in the striatum was measured by HPLC-EC method 21 days after administration. To correct for genotype-based differences in the amount of striatal DA, data are represented as percentage of the amount on the non-treated side (right striatum) of each animal (mean ± S.E.M., Tg, $n = 5$; non-Tg, $n = 5$). ***$P < 0.001$ *vs.* non-Tg by Student's t-test.

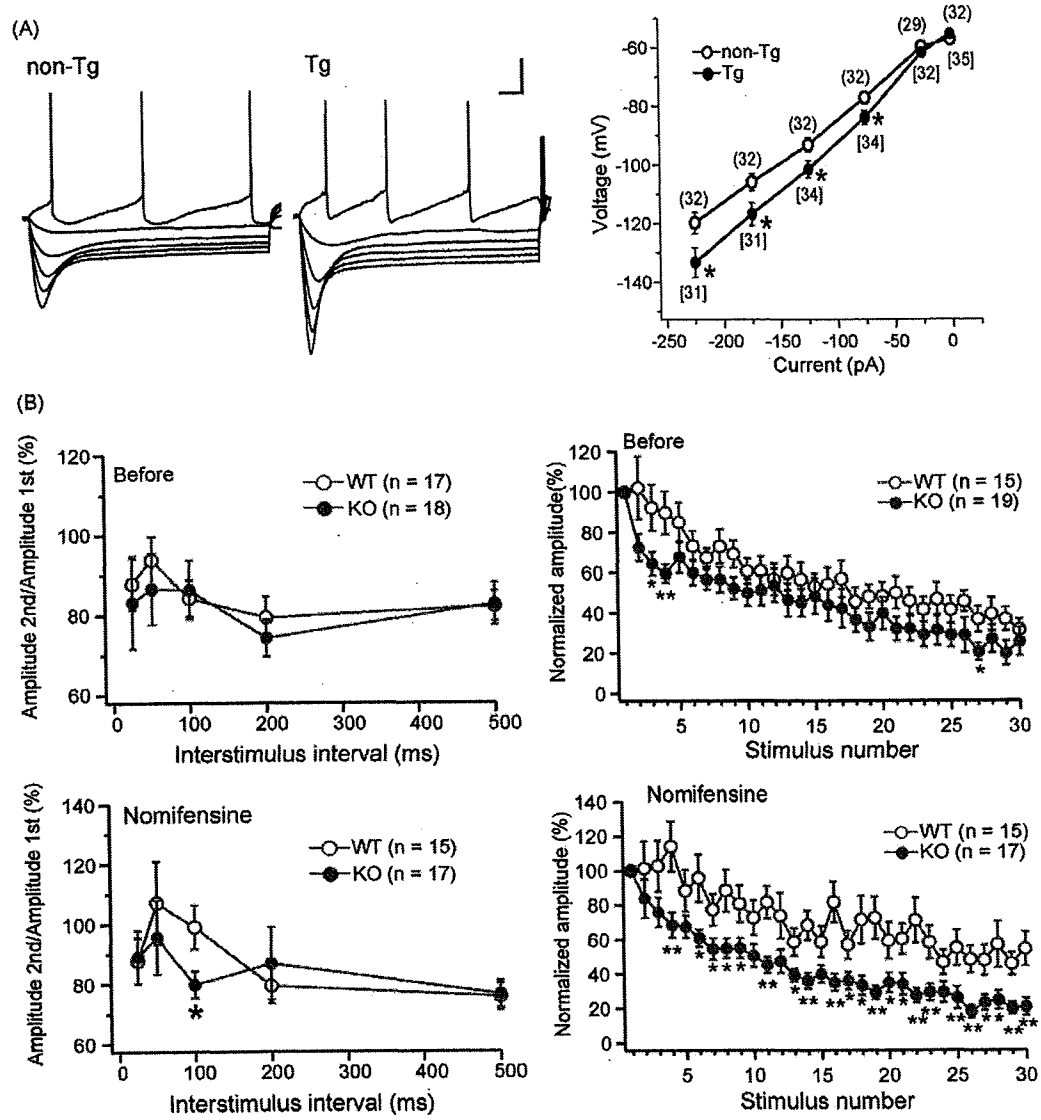

Fig. 6. Effects of Pael-R expression on physiological properties of DA neurons. (A) Sample waveforms of DA neurons taken from a non-Tg and a PrP-Tg mouse (left). Current–voltage relationships generated by injecting current pulses and recording the voltage deflections are shown on the right. Numbers in parenthesis show the numbers of cells sampled. Calibration, 25 mV, 100 ms. Input resistance in PrP-Tg mice is larger than that in non-Tg mice. *$P < 0.05$. (B) Effects of paired pulse stimulation and repeated low frequency stimulation before and after nomifensine in Pael-R KO mice. At left are shown plots of the mean (±S.E.M.) percentage of the second IPSC with respect to the first IPSC as a function of interstimulus interval before (upper) and after (lower) nomifensine application. After nomifensine treatment (3 μM), paired pulse depression (PPD) observed in wild types (WT, open circles) changed into small paired pulse facilitation (PPF), whereas PPD in knockouts (KO, gray circles) remained unchanged, yielding significant difference in paired pulse ratios at 100 ms ($P < 0.05$). Amplitudes (mean ± S.E.M.) of successive IPSCs in a burst of 30 applied 70 ms apart (i.e. at 14 Hz) normalized with respect to the amplitude of the first IPSC of the burst are shown on the right. There was a significant decrease in normalized IPSC amplitude in Pael-R KO mice (Student's *t*-test, $P < 0.05$) both before (upper) and after (lower) nomifensine treatment.

the change in DA content at this stage may be too small to detect nigrostriatal abnormalities in our electrophysiological analysis.

4. Discussion

Pael-R, transcripts of which are exclusively expressed in the CNS and testis, is a putative G protein coupled receptor (Donohue et al., 1998; Kawasawa et al., 2003). Unfolded Pael-R is thought to have a role in the etiology of AR-JP (Imai et al., 2001; Yang et al., 2003). Moreover, Pael-R-immunoreactivity has been observed in Lewy bodies of PD patients (Murakami et al., 2004). These reports suggest that unfolded Pael-R is associated with degeneration of DA neurons in PD. However, the physiological function of Pael-R in the CNS remains unknown. Our investigation of Pael-R-deficient and Pael-R Tg mice here revealed its physiological function as well as its pathological function in nigrostriatal system.

Although in Pael-R-deficient mice the number of TH-positive neurons in the SN was only slightly reduced, the striatal level of DA was significantly reduced. The alteration of DA content in these mice cannot simply be explained by a change of TH (a rate-limiting enzyme of DA synthesis, converting tyrosine into

L-DOPA) or aromatic amino acid decarboxylase (AADC, the enzyme that converts L-DOPA to dopamine) expression at protein level because the change of those expressions was not observed by Western blot analysis (data not shown). We also failed to detect a significant difference in the steady state and METH-stimulated levels of DA in the striatal CSF of Pael-R KO mice or a behavioral difference following METH administration. Thus, the reduction in whole striatal DA content could come from a non-releasable pool of DA in DA neurons.

The observations of Pael-R KO mice by Marazziti et al. (2004) is almost consistent with the results of our Pael-R KO mice. However, we do not see a significant reduction in the body weights of Pael-R KO mice and a significant defect of motor performance in the rotarod test. Another difference is their mice were supersensitive to amphetamine as assessed by locomotor activity, whereas we failed to find a significant difference in the amount of METH-stimulated DA in the CSF of Pael-R KO mice. These inconsistencies may come from tested ages of the mice and a difference in genetic backgrounds (100% C57BL/6J in this study *versus* 75% C57BL/6J and 25% 129P2/OlaHsd mixed background in the previous study by Marazziti's group). We analyzed older mice (12-month-old for measurement of body weight and rotarod test, 6–12-month-old for METH administration) compared with those (2.5–4-month-old) in Marazziti's group. As a result, a compensation for Pael-R-deficiency may go on with age.

The electrophysiological analysis was done only in young mice (3–4-week-old) for technical reasons. We found that the DA neuron and striatal MSN input resistance significantly increased in PrP-Tg mice and striatal MSN input resistance significantly decreased in Pael-R KO although the resting membrane potentials, the firing thresholds, and the amplitudes and widths of the spikes remained unchanged. This observation suggests that Pael-R may interact with certain membrane factor(s) that determine the input resistance and thereby play an important role in membrane constitution. On the other hand, the finding that PPR was not altered in either Pael-R Tg or KO mice indicates that Pael-R does not affect the GABA release machinery. However, the decrement of PPR was evident after nomifensine treatment and after repeated low frequency stimulation in Pael-R KO mice compared with WT littermates. This result indicates that the absence of Pael-R depletes available striatal DA content, which might be consistent with a very recent report that the population of the cell-surface DAT at the presynapse of Pael-R KO mice is increased by the absence of direct interaction between Pael-R and DAT (Marazziti et al., 2007). Another recent study on a candidate of Pael-R ligands has showed that Pael-R is internalized upon stimulation by a neuropeptide head activator (HA) (Rezgaoui et al., 2006). Given that Pael-R is one of DAT-associated proteins, the cell-surface DAT may be internalized together with Pael-R upon HA stimulation. That could cause the extracellular accumulation of DA. However, the observations that Pael-R KO mice and Pael-R Tg mice are respectively resistant and susceptible to DA neurotoxins suggest that there are DAT-independent mechanisms of MPTP toxicity.

Growing numbers of reports have shown that increased DA levels affect terminal degeneration of DA neurons and that DA treatment leads to cell death *in vitro* (Ben-Shachar et al., 2004; Cantuti-Castelvetri et al., 2003; Hastings et al., 1996; LaVoie and Hastings, 1999; Masserano et al., 1996; Rabinovic et al., 2000; Xu et al., 2002; Zigmond et al., 2002). Moreover, although differing from classic Lewy bodies, dopamine-dependent neuronal inclusions have been experimentally generated in mice and cultured cells treated with METH (Fornai et al., 2004). The fact that various antioxidants can prevent DA neurotoxicity suggests oxidative stress occurring during DA metabolism might damage crucial neuronal functions and reduce survival. Indeed, the aging of human brain, which is an important risk factor for PD, is closely associated with attenuated antioxidant pathways challenged by oxidative stress (Lee et al., 2000; Lu et al., 2004). Considering constitutively high DA levels might expose DA neurons to chronic oxidative stress, one can assume Pael-R Tg mice are more sensitive than WT littermates to DA neurotoxins. DA neurotoxins such as MPTP and 6-OHDA are thought to disturb the mitochondrial activity of DA neurons possibly by promoting leakage of electrons from the mitochondrial electron transfer system and thereby generating reactive oxygen species. The levels of DAT and VMAT2 are reported to determine the sensitivity of neurons to DA neurotoxins. However, the resistance of Pael-R KO mice to MPTP was not explained by cell-surface levels of DAT in the striatum, which was shown to be significantly increased in Pael-R KO mice (Marazziti et al., 2007). The examination of cell-surface DAT level of Pael-R Tg mice, therefore, will be important to elucidate whether their sensitivity to DA neurotoxins is based on DAT-dependent mechanisms involving dysregulation of DA metabolism in the future.

Our results from Pael-R mutant mice strongly suggest that the Pael-R signal regulates the amount of DA in the dopaminergic neurons and that excessive Pael-R expression renders dopaminergic neurons susceptible to chronic DA toxicity. Further analysis of Pael-R mutant mice could provide useful information on the nigrostriatal DA metabolism and therapeutic strategy of PD.

Acknowledgments

The authors would like to thank Nagatsu T. and Sawada M. for helpful discussion, Meiji Institute of Health Science for MS12, Miyazaki J.-I. for pCAGGS-Cre, Yagi T. for pDT-ApA, the Research Resource Center of the Brain Science Institute for embryo manipulation and support for these animal experiments. This work was partially supported by the Ministry of Education, Science, Sports and Culture, Grant-in-Aid for Scientific Research on Priority Areas – Advanced Brain Science Project – #15016120 to R.T., for Scientific Research (A) #14207032 to R.T., and for Young Scientists (A) #15680011 to Y.I. and a grant from the Special Postdoctoral Researcher Program of RIKEN to Y.I.

References

Bamford, N.S., Zhang, H., Schmitz, Y., Wu, N.P., Cepeda, C., Levine, M.S., Schmauss, C., Zakharenko, S.S., Zablow, L., Sulzer, D., 2004. Heterosy-

naptic dopamine neurotransmission selects sets of corticostriatal terminals. Neuron 42, 653–663.

Ben-Shachar, D., Zuk, R., Gazawi, H., Ljubuncic, P., 2004. Dopamine toxicity involves mitochondrial complex I inhibition: implications to dopamine-related neuropsychiatric disorders. Biochem. Pharmacol. 67, 1965–1974.

Betarbet, R., Sherer, T.B., Greenamyre, J.T., 2002. Animal models of Parkinson's disease. Bioessays 24, 308–318.

Borchelt, D.R., Davis, J., Fischer, M., Lee, M.K., Slunt, H.H., Ratovitsky, T., Regard, J., Copeland, N.G., Jenkins, N.A., Sisodia, S.S., Price, D.L., 1996. A vector for expressing foreign genes in the brains and hearts of transgenic mice. Genet. Anal. 13, 159–163.

Calabresi, P., Fedele, E., Pisani, A., Fontana, G., Mercuri, N.B., Bernardi, G., Raiteri, M., 1995. Transmitter release associated with long-term synaptic depression in rat corticostriatal slices. Eur. J. Neurosci. 7, 1889–1894.

Cantuti-Castelvetri, I., Shukitt-Hale, B., Joseph, J.A., 2003. Dopamine neurotoxicity: age-dependent behavioral and histological effects. Neurobiol. Aging 24, 697–706.

Centonze, D., Picconi, B., Baunez, C., Borrelli, E., Pisani, A., Bernardi, G., Calabresi, P., 2002. Cocaine and amphetamine depress striatal GABAergic synaptic transmission through D2 dopamine receptors. Neuropsychopharmacology 26, 164–175.

Centonze, D., Grande, C., Usiello, A., Gubellini, P., Erbs, E., Martin, A.B., Pisani, A., Tognazzi, N., Bernardi, G., Moratalla, R., Borrelli, E., Calabresi, P., 2003. Receptor subtypes involved in the presynaptic and postsynaptic actions of dopamine on striatal interneurons. J. Neurosci. 23, 6245–6254.

Centonze, D., Gubellini, P., Usiello, A., Rossi, S., Tscherter, A., Bracci, E., Erbs, E., Tognazzi, N., Bernardi, G., Pisani, A., Calabresi, P., Borrelli, E., 2004. Differential contribution of dopamine D2S and D2L receptors in the modulation of glutamate and GABA transmission in the striatum. Neuroscience 129, 157–166.

Chui, D.H., Tanahashi, H., Ozawa, K., Ikeda, S., Checler, F., Ueda, O., Suzuki, H., Araki, W., Inoue, H., Shirotani, K., Takahashi, K., Gallyas, F., Tabira, T., 1999. Transgenic mice with Alzheimer presenilin 1 mutations show accelerated neurodegeneration without amyloid plaque formation. Nat. Med. 5, 560–564.

Donohue, P.J., Shapira, H., Mantey, S.A., Hampton, L.L., Jensen, R.T., Battey, J.F., 1998. A human gene encodes a putative G protein-coupled receptor highly expressed in the central nervous system. Brain Res. Mol. Brain Res. 54, 152–160.

Fornai, F., Lenzi, P., Gesi, M., Soldani, P., Ferrucci, M., Lazzeri, G., Capobianco, L., Battaglia, G., De Blasi, A., Nicoletti, F., Paparelli, A., 2004. Methamphetamine produces neuronal inclusions in the nigrostriatal system and in PC12 cells. J. Neurochem. 88, 114–123.

Fumagalli, F., Gainetdinov, R.R., Valenzano, K.J., Caron, M.G., 1998. Role of dopamine transporter in methamphetamine-induced neurotoxicity: evidence from mice lacking the transporter. J. Neurosci. 18, 4861–4869.

Goldberg, M.S., Fleming, S.M., Palacino, J.J., Cepeda, C., Lam, H.A., Bhatnagar, A., Meloni, E.G., Wu, N., Ackerson, L.C., Klapstein, G.J., Gajendiran, M., Roth, B.L., Chesselet, M.F., Maidment, N.T., Levine, M.S., Shen, J., 2003. Parkin-deficient mice exhibit nigrostriatal deficits but not loss of dopaminergic neurons. J. Biol. Chem. 278, 43628–43635.

Gomi, H., Yokoyama, T., Fujimoto, K., Ikeda, T., Katoh, A., Itoh, T., Itohara, S., 1995. Mice devoid of the glial fibrillary acidic protein develop normally and are susceptible to scrapie prions. Neuron 14, 29–41.

Hastings, T.G., Lewis, D.A., Zigmond, M.J., 1996. Role of oxidation in the neurotoxic effects of intrastriatal dopamine injections. Proc. Natl. Acad. Sci. U.S.A. 93, 1956–1961.

Imai, Y., Soda, M., Takahashi, R., 2000. Parkin suppresses unfolded protein stress-induced cell death through its E3 ubiquitin–protein ligase activity. J. Biol. Chem. 275, 35661–35664.

Imai, Y., Soda, M., Inoue, H., Hattori, N., Mizuno, Y., Takahashi, R., 2001. An unfolded putative transmembrane polypeptide, which can lead to endoplasmic reticulum stress, is a substrate of Parkin. Cell 105, 891–902.

Imai, Y., Soda, M., Hatakeyama, S., Akagi, T., Hashikawa, T., Nakayama, K.I., Takahashi, R., 2002. CHIP is associated with Parkin, a gene responsible for familial Parkinson's disease, and enhances its ubiquitin ligase activity. Mol. Cell. 10, 55–67.

Itier, J.M., Ibanez, P., Mena, M.A., Abbas, N., Cohen-Salmon, C., Bohme, G.A., Laville, M., Pratt, J., Corti, O., Pradier, L., Ret, G., Joubert, C., Periquet, M., Araujo, F., Negroni, J., Casarejos, M.J., Canals, S., Solano, R., Serrano, A., Gallego, E., Sanchez, M., Denefle, P., Benavides, J., Tremp, G., Rooney, T.A., Brice, A., Garcia de Yebenes, J., 2003. Parkin gene inactivation alters behaviour and dopamine neurotransmission in the mouse. Hum. Mol. Genet. 12, 2277–2291.

Ito, S., Kato, T., Fujita, K., 1988. Covalent binding of catechols to proteins through the sulphydryl group. Biochem. Pharmacol. 37, 1707–1710.

Kaneko, S., Hikida, T., Watanabe, D., Ichinose, H., Nagatsu, T., Kreitman, R.J., Pastan, I., Nakanishi, S., 2000. Synaptic integration mediated by striatal cholinergic interneurons in basal ganglia function. Science 289, 633–637.

Kawasawa, Y., McKenzie, L.M., Hill, D.P., Bono, H., Yanagisawa, M., 2003. G protein-coupled receptor genes in the FANTOM2 database. Genome Res. 13, 1466–1477.

Kitada, T., Asakawa, S., Hattori, N., Matsumine, H., Yamamura, Y., Minoshima, S., Yokochi, M., Mizuno, Y., Shimizu, N., 1998. Mutations in the parkin gene cause autosomal recessive juvenile parkinsonism. Nature 392, 605–608.

LaVoie, M.J., Hastings, T.G., 1999. Dopamine quinone formation and protein modification associated with the striatal neurotoxicity of methamphetamine: evidence against a role for extracellular dopamine. J. Neurosci. 19, 1484–1491.

Lee, C.K., Weindruch, R., Prolla, T.A., 2000. Gene-expression profile of the ageing brain in mice. Nat. Genet. 25, 294–297.

Lu, T., Pan, Y., Kao, S.Y., Li, C., Kohane, I., Chan, J., Yankner, B.A., 2004. Gene regulation and DNA damage in the ageing human brain. Nature 429, 883–891.

Marazziti, D., Gallo, A., Golini, E., Matteoni, R., Tocchini-Valentini, G.P., 1998. Molecular cloning and chromosomal localization of the mouse Gpr37 gene encoding an orphan G-protein-coupled peptide receptor expressed in brain and testis. Genomics 53, 315–324.

Marazziti, D., Golini, E., Mandillo, S., Magrelli, A., Witke, W., Matteoni, R., Tocchini-Valentini, G.P., 2004. Altered dopamine signaling and MPTP resistance in mice lacking the Parkinson's disease-associated GPR37/parkin-associated endothelin-like receptor. Proc. Natl. Acad. Sci. U.S.A. 101, 10189–10194.

Marazziti, D., Mandillo, S., Di Pietro, C., Golini, E., Matteoni, R., Tocchini-Valentini, G.P., 2007. GPR37 associates with the dopamine transporter to modulate dopamine uptake and behavioral responses to dopaminergic drugs. Proc. Natl. Acad. Sci. U.S.A. 104, 9846–9851.

Masserano, J.M., Gong, L., Kulaga, H., Baker, I., Wyatt, R.J., 1996. Dopamine induces apoptotic cell death of a catecholaminergic cell line derived from the central nervous system. Mol. Pharmacol. 50, 1309–1315.

Murakami, T., Shoji, M., Imai, Y., Inoue, H., Kawarabayashi, T., Matsubara, E., Harigaya, Y., Sasaki, A., Takahashi, R., Abe, K., 2004. Pael-R is accumulated in Lewy bodies of Parkinson's disease. Ann. Neurol. 55, 439–442.

Nelson, E.L., Liang, C.L., Sinton, C.M., German, D.C., 1996. Midbrain dopaminergic neurons in the mouse: computer-assisted mapping. J. Comp. Neurol. 369, 361–371.

Rabinovic, A.D., Lewis, D.A., Hastings, T.G., 2000. Role of oxidative changes in the degeneration of dopamine terminals after injection of neurotoxic levels of dopamine. Neuroscience 101, 67–76.

Rezgaoui, M., Susens, U., Ignatov, A., Gelderblom, M., Glassmeier, G., Franke, I., Urny, J., Imai, Y., Takahashi, R., Schaller, H.C., 2006. The neuropeptide head activator is a high-affinity ligand for the orphan G-protein-coupled receptor GPR37. J. Cell. Sci. 119, 542–549.

Shimura, H., Hattori, N., Kubo, S., Mizuno, Y., Asakawa, S., Minoshima, S., Shimizu, N., Iwai, K., Chiba, T., Tanaka, K., Suzuki, T., 2000. Familial Parkinson disease gene product, parkin, is a ubiquitin–protein ligase. Nat. Genet. 25, 302–305.

Sunaga, S., Maki, K., Komagata, Y., Ikuta, K., Miyazaki, J.I., 1997. Efficient removal of loxP-flanked DNA sequences in a gene-targeted locus by transient expression of Cre recombinase in fertilized eggs. Mol. Reprod. Dev. 46, 109–113.

Tateno, M., Sadakata, H., Tanaka, M., Itohara, S., Shin, R.M., Miura, M., Masuda, M., Aosaki, T., Urushitani, M., Misawa, H., Takahashi, R., 2004. Calcium-permeable AMPA receptors promote misfolding of mutant SOD1 protein and development of amyotrophic lateral sclerosis in a transgenic mouse model. Hum. Mol. Genet. 13, 2183–2196.

Valdenaire, O., Giller, T., Breu, V., Ardati, A., Schweizer, A., Richards, J.G., 1998. A new family of orphan G protein-coupled receptors predominantly expressed in the brain. FEBS Lett. 424, 193–196.

West, M.J., 1999. Stereological methods for estimating the total number of neurons and synapses: issues of precision and bias. Trends Neurosci. 22, 51–61.

Wieczorek, W.J., Kruk, Z.L., 1994. A quantitative comparison on the effects of benztropine, cocaine and nomifensine on electrically evoked dopamine overflow and rate of re-uptake in the caudate putamen and nucleus accumbens in the rat brain slice. Brain Res. 657, 42–50.

Xu, J., Kao, S.Y., Lee, F.J., Song, W., Jin, L.W., Yankner, B.A., 2002. Dopamine-dependent neurotoxicity of alpha-synuclein: a mechanism for selective neurodegeneration in Parkinson disease. Nat. Med. 8, 600–606.

Yanagawa, Y., Kobayashi, T., Ohnishi, M., Tamura, S., Tsuzuki, T., Sanbo, M., Yagi, T., Tashiro, F., Miyazaki, J., 1999. Enrichment and efficient screening of ES cells containing a targeted mutation: the use of DT-A gene with the polyadenylation signal as a negative selection maker. Transgenic Res. 8, 215–221.

Yang, Y., Nishimura, I., Imai, Y., Takahashi, R., Lu, B., 2003. Parkin suppresses dopaminergic neuron-selective neurotoxicity induced by Pael-R in *Drosophila*. Neuron 37, 911–924.

Zhang, Y., Gao, J., Chung, K.K., Huang, H., Dawson, V.L., Dawson, T.M., 2000. Parkin functions as an E2-dependent ubiquitin–protein ligase and promotes the degradation of the synaptic vesicle-associated protein, CDCrel-1. Proc. Natl. Acad. Sci. U.S.A. 97, 13354–13359.

Zhou, Q.Y., Palmiter, R.D., 1995. Dopamine-deficient mice are severely hypoactive, adipsic, and aphagic. Cell 83, 1197–1209.

Zigmond, M.J., Hastings, T.G., Perez, R.G., 2002. Increased dopamine turnover after partial loss of dopaminergic neurons: compensation or toxicity? Parkinsonism Relat. Disord. 8, 389–393.

BRIEF COMMUNICATIONS

nature neuroscience

Astrocytes as determinants of disease progression in inherited amyotrophic lateral sclerosis

Koji Yamanaka[1,2], Seung Joo Chun[1], Severine Boillee[1], Noriko Fujimori-Tonou[2], Hirofumi Yamashita[2], David H Gutmann[3], Ryosuke Takahashi[4], Hidemi Misawa[5] & Don W Cleveland[1]

Dominant mutations in superoxide dismutase cause amyotrophic lateral sclerosis (ALS), an adult-onset neurodegenerative disease that is characterized by the loss of motor neurons. Using mice carrying a deletable mutant gene, diminished mutant expression in astrocytes did not affect onset, but delayed microglial activation and sharply slowed later disease progression. These findings demonstrate that mutant astrocytes are viable targets for therapies for slowing the progression of non–cell autonomous killing of motor neurons in ALS.

ALS is an adult-onset neurodegenerative disease, characterized by a progressive and fatal loss of motor neurons. Dominant mutations in the gene for superoxide dismutase (*SOD1*) are the most frequent cause of inherited ALS. Ubiquitous expression of mutant *SOD1* in rodents leads to progressive, selective motor neuron degeneration as a result of acquired toxic properties. The exact mechanism responsible for motor neuron degeneration in ALS, however, is not known[1,2]. Mutant damage in the vulnerable motor neurons is a key determinant of disease onset[3], whereas accumulating evidence supports an active role of non-neuronal cells in motor neuron degeneration[3–7]. Evidence with selective gene excision[3] or bone-marrow grafting[5] has demonstrated that mutant SOD1-derived damage in microglia accelerates later disease progression. Despite the importance of astrocyte function, the role of mutant action in astrocytes in disease has not been tested *in vivo*.

To examine whether mutant SOD1 damage in astrocytes contributes to disease, *loxSOD1*^{G37R} mice[3], carrying a mutant *SOD1* gene that can be deleted by the action of the Cre recombinase, were mated with *GFAP-Cre* mice (**Fig. 1** and **Supplementary Fig. 1** online), which express both Cre recombinase and β-galactosidase (*LacZ*) under the control of the human GFAP promoter[8]. Mice from these matings that carry the *GFAP-Cre* transgene are denoted as Cre$^+$, whereas mice without it are referred to as Cre$^-$. To determine the cell-type specificity of Cre expression in the spinal cord, *GFAP-Cre* mice were mated to Rosa26 mice, which ubiquitously express a *LacZ* gene that encodes functional β-galactosidase only after Cre-mediated recombination. Although this *GFAP-Cre* transgene is expressed in a subset of neurons in the cerebellum and hippocampus during embryogenesis[9], measurement of β-galactosidase activity (by deposition of a blue reaction product after addition of the X-gal substrate) demonstrated that Cre expression and Cre-mediated recombination was restricted in the spinal cord to GFAP-reactive astrocytes (**Fig. 1a,b**). The efficiency of mutant gene excision in cultured astrocytes from newborn *loxSOD1*^{G37R}*/GFAP-Cre*$^+$ mice was ~76% (**Fig. 1d,e**), determined by quantitative PCR for human SOD1 transgene number (**Fig. 1d**) and immunoblotting for mutant SOD1 levels (**Fig. 1e**). We observed neither detectable Cre activity nor mutant gene excision in microglia (**Fig. 1c** and **Supplementary Fig. 2** online).

A simple, objective measure of disease onset and early disease was applied by initiation of weight loss, itself reflecting denervation-induced muscle atrophy. Reduction of SOD1^{G37R} in astrocytes did not slow disease onset nor early disease (GFAP-Cre$^+$, 341.6 ± 48.9 d; GFAP-Cre$^-$, 337.0 ± 35.8 d; **Fig. 1f,h**). However, late disease progression (from early disease to end stage) was sharply delayed, providing a mean extension of survival by 48 d (Cre$^+$, 87.4 d; Cre$^-$, 39.5 d; **Fig. 1j**). Progression from onset to early disease was more modestly slowed by 14 d (Cre$^+$, 99.3 d; Cre$^-$, 85.2 d; **Fig. 1i**). Overall survival was extended by 60 d (Cre$^+$, 436.5 ± 38.8 d; Cre$^-$, 376.5 ± 26.9 d; **Fig. 1g**). This contrasts with delayed disease onset from diminished mutant synthesis solely within motor neurons (with a *VAChT-Cre* transgene carrying the motor neuron–specific vesicular acetylcholine transporter promoter) without affecting disease progression (**Supplementary Results, Supplementary Methods** and **Supplementary Fig. 3** online), just as reported previously with an *Isl1* (*Islet1*)*-Cre* transgene that is expressed in motor neurons and some peripheral tissues[3].

Astrocytic and microglial cell activation is a well-accepted feature of SOD1 mutant–mediated ALS[1,2]. An elevated proportion of GFAP-positive astrocytes appeared before disease onset (**Fig. 2a**) in *loxSOD1*^{G37R} mice. This astrogliosis was progressive, readily apparent by onset (**Fig. 2b**) and more prominent during disease progression (**Fig. 2c**). Despite substantial mutant reduction, astrogliosis was not, however, different in comparing disease-matched *loxSOD1*^{G37R}*/GFAP-Cre*$^+$ mice (**Fig. 2d,e**) and *loxSOD1*^{G37R}*/GFAP-Cre*$^-$ mice (**Fig. 2b,c**).

Microglial activation occurred at earliest disease onset in *Cre*$^-$ mice (**Fig. 2g**) and was progressively more prominent during disease progression (**Fig. 2h**). Microglial activation was, however, substantially delayed from onset through early disease in the *GFAP-Cre*$^+$ mice when mutant SOD1 levels were reduced only in astrocytes (**Fig. 2i,j**). By exploiting the presence of β-galactosidase to mark astrocytes with diminished SOD1 mutant synthesis, examination of sections throughout lumbar spinal cords of symptomatic *loxSOD1*^{G37R}*/GFAP-Cre*$^+$ mice

[1]Ludwig Institute for Cancer Research and Department of Medicine and Neuroscience, University of California at San Diego, 9500 Gilman Drive, La Jolla, California 92093-0670, USA. [2]Yamanaka Research Unit, RIKEN Brain Science Institute, 2-1 Hirosawa, Wako, Saitama 351-0198, Japan. [3]Department of Neurology, Washington University School of Medicine, 660 South Euclid Avenue, St. Louis, Missouri 63110, USA. [4]Department of Neurology, Graduate School of Medicine, Kyoto University, 54 Shogoin Kawahara-cho, Sakyo-ku, Kyoto 606-8507, Japan. [5]Department of Pharmacology, Kyoritsu University of Pharmacy, 1-5-30 Shibakoen, Minato-ku, Tokyo 105-8512, Japan. Correspondence should be addressed to D.W.C. (dcleveland@ucsd.edu) or K.Y. (kyamanaka@brain.riken.jp).

Received 26 November 2007; accepted 7 January 2008; published online 3 February 2008; doi:10.1038/nn2047

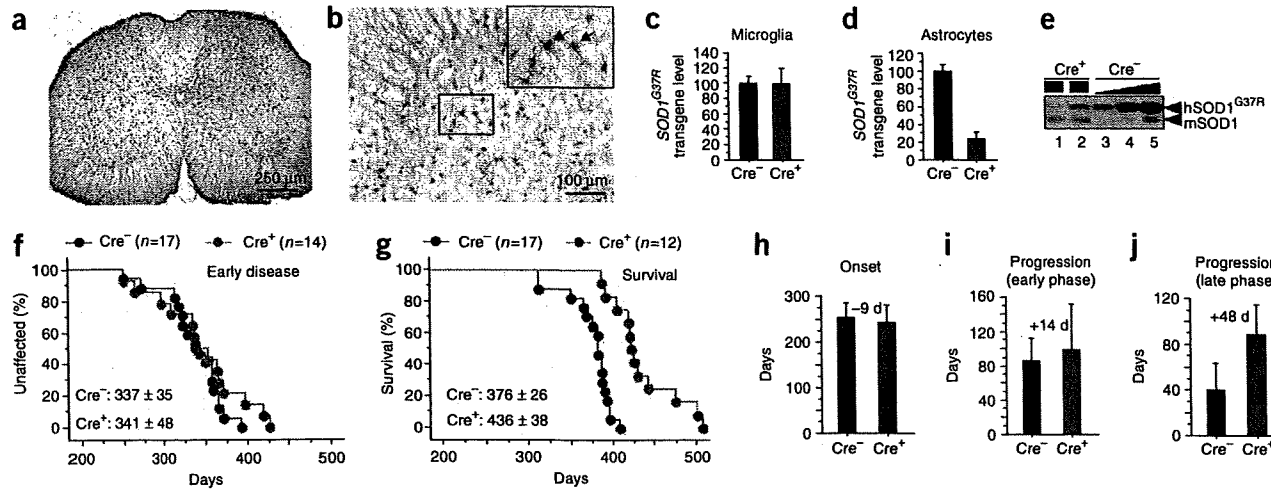

Figure 1 Selective Cre-mediated gene excision shows that mutant SOD1 action in astrocytes is a primary determinant of late disease progression. (**a**,**b**) β-galactosidase (β-gal) activity in astrocytes in whole (**a**) or in the anterior horn region (**b**) of the lumbar spinal cord section of *GFAP-Cre*/Rosa26 reporter mice visualized with X-gal and immunostaining with GFAP antibody. Inset, magnified image of the boxed area in **b**. Arrows indicate β-gal/GFAP-Cre–expressing astrocytes. (**c**,**d**) *loxSOD1*^{G37R} transgene levels ($n = 3$ for each group) in primary microglia (**c**) or astrocytes (**d**) from *loxSOD1*^{G37R}/*GFAP-Cre*$^{+}$ and *loxSOD1*^{G37R} mice using real-time PCR. (**e**) We determined SOD1^{G37R} and mouse SOD1 levels by immunoblotting extracts from isolated primary astrocytes of *loxSOD1*^{G37R}/*GFAP-Cre*$^{+}$ (lanes 1, 2) and a dilution series of a comparable extract from LoxSOD1^{G37R} astrocytes representing 25%, 50% and 100% of the protein amounts loaded in lanes 1 and 2 (lanes 3–5). (**f**,**g**) Ages at which early disease phase (to 10% weight loss, $P = 0.76$; **f**) or end-stage disease ($P < 0.0001$; **g**) were reached for *loxSOD1*^{G37R}/*GFAP-Cre*$^{+}$ mice (red) and *loxSOD1*^{G37R} littermates (blue). Mean ages ± s.d. are provided. (**h**–**j**) Mean onset ($P = 0.47$) (**h**), mean duration of early disease (from onset to 10% weight loss, $P = 0.35$; **i**) and a late disease (from 10% weight loss to end stage, $P < 0.0001$; **j**) for *loxSOD1*^{G37R}/*GFAP-Cre*$^{+}$ (red) and *loxSOD1*^{G37R} littermates (blue). At each time point, *P* value was determined by unpaired *t*-test. Error bars denote s.d.

revealed an inverse relationship (**Fig. 3a–g**) between the number of astrocytes with reduced mutant SOD1 (*Cre*$^{+}$) and activated microglia (correlation coefficient, $r = -0.868$, $P < 0.001$), despite comparable astrocytic activation. Thus, microglial activation was most prominent in areas with the highest mutant SOD1–expressing astrocyte concentration.

Elevated production of nitric oxide by upregulated inducible nitric oxide synthase (iNOS) has been reported in mutant SOD1 mice[10], although deletion of the iNOS gene has modest[11] or no[12] effect on SOD1-mediated disease. It is not known in which glial cells this nitric oxide is produced in *in vivo* models of ALS, although both microglia and astrocytes have an ability to produce it when stimulated *in vitro*[13]. Triple staining of lumbar spinal cord sections with iNOS, Mac2 and GFAP antibodies (**Fig. 3h–r**) revealed that almost all iNOS-positive cells were Mac2-positive microglia (**Fig. 3n–r** and **Supplementary Fig. 4** online), indicating that activated microglia are the primary cell type producing nitric oxide in this SOD1 mouse model. Diminishing mutant synthesis in astrocytes inhibited iNOS induction in disease-matched, symptomatic SOD1 mice (**Fig. 3h,k**), consistent with substantial inhibition of microglial activation (**Fig. 3i,l**).

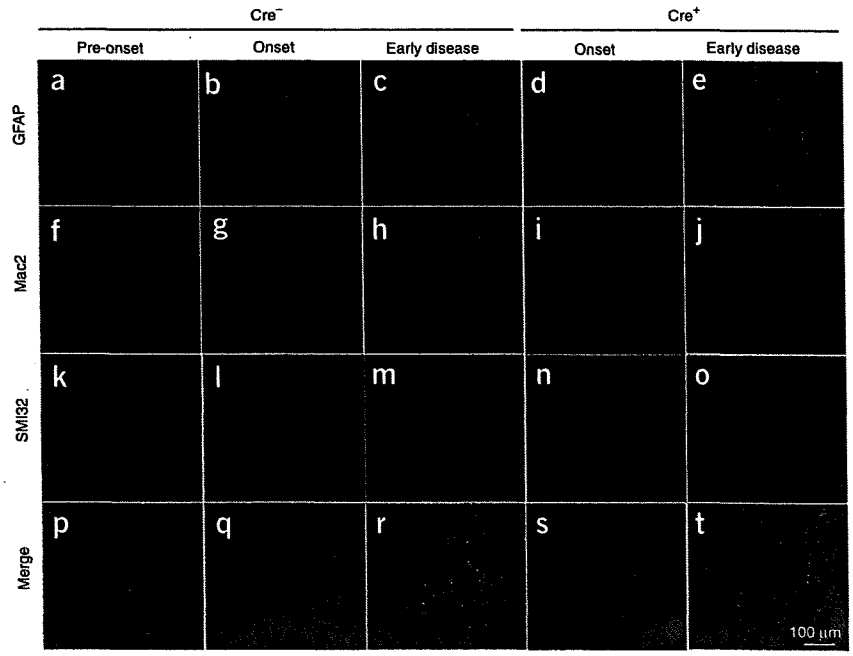

Figure 2 Selective downregulation of mutant SOD1 in astrocytes significantly inhibits microglial activation. (**a**–**t**) GFAP-positive astrocytes (**a**–**e**), Mac2-positive activated microglia (**f**–**j**) and motor neurons identified with the neurofilament antibody SMI-32 (**k**–**o**) in the lumbar spinal cord of a *loxSOD1*^{G37R} mouse before disease onset (**a**,**f**,**k**,**p**), at disease onset (**b**,**g**,**l**,**q**) or during early disease (**c**,**h**,**m**,**r**), together with *loxSOD1*^{G37R}/*GFAP-Cre*$^{+}$ mice at disease onset (**d**,**i**,**n**,**s**) or during early disease (**e**,**j**,**o**,**t**). Merged images are shown in **p**–**t**.

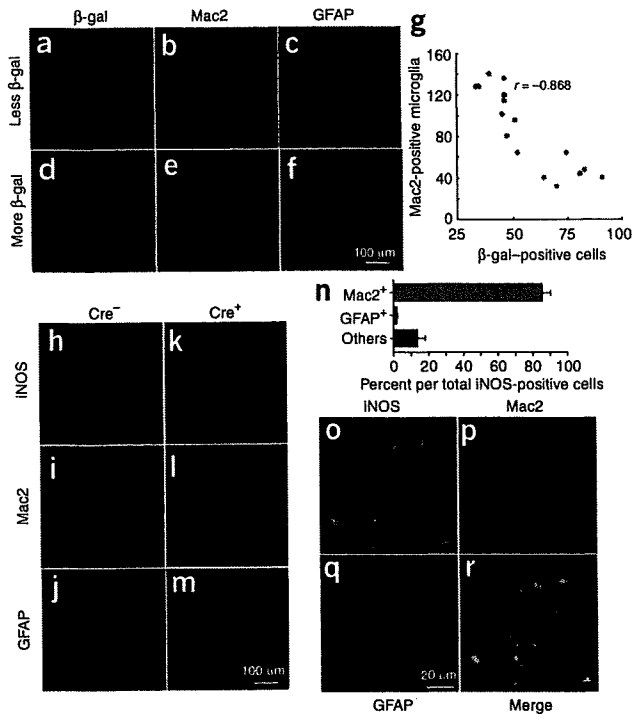

Figure 3 Mutant-expressing astrocytes enhance microglial activation and induction of iNOS. (**a–f**) Images of β-galactosidase (**a,d**), Mac2 (**b,e**) and GFAP (**c,f**) staining from a left (**a–c**) and right (**d–f**) lumbar spinal cord section from a 12-month-old *loxSOD1*^{G37R}*/GFAP-Cre*$^{+}$ mouse. *GFAP-Cre*$^{+}$ astrocytes are marked by β-galactosidase (**a,d**). (**g**) Inverted correlation between the number of Cre-positive astrocytes and Mac2-positive microglia in *loxSOD1*^{G37R}*/GFAP-Cre*$^{+}$ mice lumbar spinal cord sections (correlation coefficient, $r = -0.868$, $P < 0.001$). (**h–m**) Lumbar spinal cord sections from *loxSOD1*^{G37R} (**h–j**) and *loxSOD1*^{G37R}*/GFAP-Cre*$^{+}$ (**k–m**) mice at the early disease stage immunostained with antibodies to iNOS (**h,k**), Mac2 (**i,l**), and GFAP (**j,m**). (**n**) Quantification of iNOS-positive cells in the anterior horn from lumbar spinal cord of symptomatic *loxSOD1*^{G37R} mice. We plotted the averaged percent of iNOS^{+}/Mac2^{+} (red), iNOS^{+}/GFAP^{+} (blue) and iNOS^{+}/other cell type (black) per total iNOS^{+} cells. (**o–r**) Magnified images of anterior horn from lumbar spinal cord of symptomatic *loxSOD1*^{G37R} mice stained with iNOS (**o**), Mac2 (**p**) and GFAP (**q**). Merged image illustrates that iNOS-positive cells are Mac2-positive microglia (**r**).

A role for astrocytes in inherited ALS has been previously considered in several contexts. Mutant-expressing astrocytes produce and release one or more as yet uncharacterized components that can accelerate motor neuron death *in vitro*[6,7]. Focal loss of the astrocytic EAAT2 glutamate transporter in affected regions[14] (**Supplementary Fig. 5** online) and the failure of normal glutamate uptake of *SOD1*^{G93A} astrocytes *in vitro*[15] support glutamate-dependent excitotoxicity as a component of disease. Nevertheless, diminished mutant SOD1 synthesis in most astrocytes did not affect disease-dependent loss of EAAT2 from those astrocytes (**Supplementary Fig. 5**), indicating that a reduction in glutamate transport reflects non–cell autonomous damage to astrocytes, in part, from mutant SOD1 synthesized by other cells. Our use of selective gene excision has now demonstrated that mutant SOD1 damage in both microglia[3] and astrocytes (**Fig. 1g–j**) accelerates later disease progression without affecting the initiation of motor neuron degeneration and phenotypic disease onset. Discovery that damage in astrocytes determines the timing of microglial activation and infiltration provides further evidence that, beyond any direct effect of mutant astrocytes on motor neurons, such astrocytes amplify an inflammatory response from microglia (including enhanced production of nitric oxide and possibly of toxic cytokines), leading to further damage to the motor neurons and accelerated disease progression through a non–cell autonomous mechanism (**Supplementary Fig. 6** online). These findings validate therapies, including astrocytic stem cell–replacement approaches, that aim to slow disease progression in ALS by supplementing healthy astrocytes or modulating toxicity in astrocytes to control an inflammatory response of microglia.

Note: Supplementary information is available on the Nature Neuroscience website.

ACKNOWLEDGMENTS

This work was supported by a US National Institutes of Health grant (NS 27036) and a grant from the Packard ALS Center at Johns Hopkins (D.W.C.), as well as a Muscular Dystrophy Association developmental grant, the Uehara Memorial Foundation, the Nakabayashi Trust for ALS Research and a grant-in-aid for Scientific Research (19591021) and on Priority Area (19044048) from the Ministry of Education, Culture, Sports, Science and Technology of Japan (K.Y.). Salary support for D.W.C is provided by the Ludwig Institute for Cancer Research. S.B. is a recipient of a Fondation pour la Recherche Medical fellowship, an Institut National de la santé et de la Recherché Medicale fellowship and a Muscular Dystrophy Association developmental grant.

AUTHOR CONTRIBUTIONS

K.Y., S.J.C., S.B., N.F.-T. and H.Y. conducted the experiments. D.H.G., R.T. and H.M. provided essential experimental tools and advice. K.Y., S.B., and D.W.C. were responsible for the overall design of the project, analyses of the results and writing the manuscript.

Published online at http://www.nature.com/natureneuroscience
Reprints and permissions information is available online at http://npg.nature.com/reprintsandpermissions

1. Pasinelli, P. & Brown, R.H. *Nat. Rev. Neurosci.* **7**, 710–723 (2006).
2. Boillee, S., Vande Velde, C. & Cleveland, D.W. *Neuron* **52**, 39–59 (2006).
3. Boillee, S. *et al. Science* **312**, 1389–1392 (2006).
4. Clement, A.M. *et al. Science* **302**, 113–117 (2003).
5. Beers, D.R. *et al. Proc. Natl. Acad. Sci. USA* **103**, 16021–16026 (2006).
6. Di Giorgio, F.P., Carrasco, M.A., Siao, M.C., Maniatis, T. & Eggan, K. *Nat. Neurosci.* **10**, 608–614 (2007).
7. Nagai, M. *et al. Nat. Neurosci.* **10**, 615–622 (2007).
8. Bajenaru, M.L. *et al. Mol. Cell. Biol.* **22**, 5100–5113 (2002).
9. Fraser, M.M. *et al. Cancer Res.* **64**, 7773–7779 (2004).
10. Almer, G., Vukosavic, S., Romero, N. & Przedborski, S. *J. Neurochem.* **72**, 2415–2425 (1999).
11. Martin, L.J. *et al. J. Comp. Neurol.* **500**, 20–46 (2007).
12. Son, M., Fathallah-Shaykh, H.M. & Elliott, J.L. *Ann. Neurol.* **50**, 273 (2001).
13. Barbeito, L.H. *et al. Brain Res. Brain Res. Rev.* **47**, 263–274 (2004).
14. Howland, D.S. *et al. Proc. Natl. Acad. Sci. USA* **99**, 1604–1609 (2002).
15. Vermeiren, C. *et al. J. Neurochem.* **96**, 719–731 (2006).

Available online at www.sciencedirect.com
ScienceDirect
Neuroscience Research xxx (2008) xxx–xxx
Neuroscience Research
www.elsevier.com/locate/neures

L347P PINK1 mutant that fails to bind to Hsp90/Cdc37 chaperones is rapidly degraded in a proteasome-dependent manner

Yasuhiro Moriwaki [a,b], Yeon-Jeong Kim [b], Yukari Ido [a], Hidemi Misawa [a], Koichiro Kawashima [a], Shogo Endo [c], Ryosuke Takahashi [b,d,*]

[a] *Department of Pharmacology, Kyoritsu University of Pharmacy, 1-5-30 Shibakoen, Minato-ku, Tokyo 105-8512, Japan*
[b] *Laboratory for Motor System Neurodegeneration, RIKEN Brain Science Institute, 2-1 Hiroswa, Wako-Shi, Saitama 351-0198, Japan*
[c] *Unit for Molecular Neurobiology of Learning and Memory, Initial Research Project, Okinawa Institute of Science and Technology, Uruma, Okinawa 904-2234, Japan*
[d] *Department of Neurology, Kyoto University Graduate School of Medicine, 54 Kawahara-cho, Shogoin, Sakyo-ku, Kyoto 606-8507, Japan*

Received 26 November 2007; accepted 15 January 2008

Abstract

Mutation of PTEN-induced kinase 1 (*PINK1*), which encodes a putative mitochondrial serine/threonine kinase, leads to PARK6, an autosomal recessive form of familial Parkinson's disease. Although the precise function(s) of PINK1 protein is unknown, the recessive inheritance of this form of Parkinson's disease suggests loss of PINK1 function is closely associated with its pathogenesis. Here we report that PINK1 forms a complex with the molecular chaperones Hsp90 and Cdc37/p50 within cells, which appears to enhance its stability. When cells were treated with an Hsp90 inhibitor (geldanamycin or novobiocin), levels of PINK1 were greatly diminished, reflecting its rapid degradation via ubiquitin-proteasome pathway. Similarly, the half-life of a pathogenic PINK1 mutant (L347P) that did not interact with Hsp90 or Cdc37/p50 was only 30 min, whereas that of wild-type PINK1 was 1 h. These results strongly suggest that Hsp90 and Cdc37 are binding partners of PINK1 which regulate its stability.

Keywords: Parkinson's disease; PINK1; Hsp90; Cdc37; Proteasome; Stability

1. Introduction

Parkinson's disease (PD) is the second most frequently occurring neurodegenerative disorder and is characterized by selective dopaminergic neural cell loss in the substantia nigra (Dauer and Przedborski, 2003). Most cases of PD are sporadic; in 5–10% of the PD patients, however, the cause is an inherited gene mutation. Moreover, the fact that the clinical characteristics of familial PD are similar to those of sporadic PD has lead to efforts to understand the pathogenic mechanisms induced by the related gene mutations. Several genes are now known to be causally associated with familial PD (Abou-Sleiman et al., 2006). Among them, mutations in the PTEN-induced putative kinase 1 gene (*PINK1*) have been shown to be associated with an autosomal recessive form of familial PD (Valente et al., 2004).

PINK1 was initially isolated from endometrial cancer cells overexpressing PTEN (Unoki and Nakamura, 2001), and the predicted primary sequence of PINK1 protein included an N-terminal mitochondrial-targeting signal along with a catalytic serine/threonine kinase domain. Although PINK1's mitochondrial localization and self-directed phosphorylation activity have already been characterized (Valente et al., 2004; Beilina et al., 2005; Silvestri et al., 2005; Nakajima et al., 2003), its relation to the pathogenesis of PD is poorly understood. However, evidence from several recent studies suggests that PINK1 has the ability to protect cells from stress-induced mitochondrial dysfunction and apoptosis (Valente et al., 2004; Petit et al., 2005; Deng et al., 2005; Park et al., 2006; Clark et al., 2006; Tang et al., 2006). In addition, Deng et al. (2005) recently showed that suppression of PINK1 expression reduces cell viability and significantly increases 1-methyl-4-phenylpyridinium (MPP^+)- and rotenone-induced cytotoxicity. Consistent with those findings, *PINK1*-null flies exhibit male sterility,

* Corresponding author at: Department of Neurology, Kyoto University Graduate School of Medicine, 54 Kawahara-cho, Shogoin, Sakyo-ku, Kyoto 606-8507, Japan. Tel.: +81 75 751 3770; fax: +81 75 761 9780.
E-mail address: ryosuket@kuhp.kyoto-u.ac.jp (R. Takahashi).

0168-0102/$ – see front matter
doi:10.1016/j.neures.2008.01.006

apoptotic muscle degeneration, defects in mitochondrial morphology and increased sensitivity to multiple stresses, including oxidative stress (Park et al., 2006; Clark et al., 2006). These data, along with the recessive nature of *PINK1* mutations, suggest that this form of familial PD is associated with the loss of PINK1 function.

On the other hand, Tang et al. (2006) showed that DJ-1, another protein causatively associated with familial PD, normally interacts with and stabilizes PINK1, and DJ-1 mutations that attenuate this interaction reduce the stability of PINK1. These findings suggest that protein–protein interactions between PINK1 and one or more unknown proteins could play a key regulatory role in affecting the activity and stability of PINK1. In the present study, therefore, we endeavored to isolate PINK1-binding partners using a combination of immunoprecipitation and mass-spectrometric analysis with the aim of obtaining additional information on the pathogenic features of PINK1 mutations. Our findings suggest that the stability of PINK1 is strongly affected by its interaction with Hsp90, and that inhibition of the PINK1–Hsp90 interaction might contribute to the pathogenesis of PD.

2. Materials and methods

2.1. Plasmids and antibodies

The coding region of human PINK1 was cloned using standard RT-PCR techniques. PINK1 mutants were generated using a QuikChange site-directed mutagenesis kit (Stratagene) according to the manufacturer's instructions. Wild-type and all mutant PINK1 cDNAs were cloned into the mammalian expression vector pcDNA3, which also contained the FLAG tag sequence at its 3′ terminal (pcDNA3-FLAG-C). Proper construction of all the plasmids was verified by DNA sequencing. Anti-FLAG (M2), anti-Hsp90 (H-114), anti-Cdc37 (C-11) and anti-HA (Y-11) Abs were purchased from Sigma or Santa Cruz.

2.2. Cell culture and transfection

COS7 and HEK293 cells were cultured in Dulbecco's modified Eagle's medium supplemented with 10% heat-inactivated fetal bovine serum (ICN Biomedical, Inc.), 50 U/ml of penicillin and 50 U/ml of streptomycin at 37 °C under an atmosphere of 95% air/5% CO_2. Plasmids encoding PINK1 cDNAs were transfected into cells using Lipofectamine or Lipofectamine 2000 (Invitrogen) according to the manufacturer's instructions.

2.3. Purification of PINK1-binding proteins

PINK1-FLAG-transfected HEK293 cells were homogenized in lysis buffer (20 mM Hepes [pH 7.4], 150 mM NaCl, 10% glycerol and 1% Triton X-100) supplemented with Complete Protease Inhibitors (Roche Diagnostics). The soluble fraction of the lysate was immunoprecipitated with anti-FLAG M2 agarose (Sigma) and then washed five times in lysis buffer without protease inhibitors. The fractions eluted with 200 μg/ml FLAG peptide were resolved by SDS-PAGE, after which the protein bands were stained with Coomassie Brilliant Blue (CBB) and excised for in-gel digestion.

2.4. Mass-spectral analysis

In-gel digestion was carried out as described by Mineki et al. (2002). Briefly, the excised protein bands were alkylated and then incubated with 12.5 ng/μl trypsin/100 mM NH_4HCO_3 overnight at 37 °C. The resultant tryptic peptides were extracted from the gel by successive incubations with (i) 50% CH_3CN/1% trifluoroacetic acid and (ii) 20% HCOOH/25% CH_3CN/15% isopropanol/40% H_2O. The extracts from each step were pooled and dried by vacuum centrifugation. For peptide mapping, we used a LCQ-Deca XP ion trap mass spectrometer with a nanoelectrospray ionization source (Thermo Electron Corp., Waltham, MA) combined with a reverse-phase capillary column (Cadenza C18, 2 mm × 50 mm, Microme BioResources, Inc., Auburn, CA) on a Magic 2002 high performance liquid chromatography system (Microme BioResources, Inc.). The MS spectra and MS/MS spectra data were collected using Xcalibur software (Matrix Science, London, UK). The data were analyzed for candidate sequences of PINK1-interacting proteins using MASCOT software (Matrix Science) with a public domain protein database (National Center for Biotechnology Information).

2.5. Treatment with Hsp90 and protease inhibitors

Geldanamycin (GA) and novobiocin were purchased from Sigma. Epoxomycin, benzyloxycarbonyl-Leu-Leu-Leu-aldehyde (MG132), pepstatin A and leupeptin were from Peptide Institute. GA (1 mM) was prepared in DMSO and used at a final concentration of 3 μM; novobiocin was prepared in water and used at a final concentration of 1 mM; MG132 (10 mM) was prepared in DMSO and used at a final concentration of 5 μM; epoxomycin (1 mM) was prepared in DMSO and used at a final concentration of 1 μM; leupeptin (1 mM) was prepared in water and used at a final concentration of 20 μM; and pepstatin (1 mM) was prepared in DMSO and used at a final concentration of 25 μM. Cells were exposed to drugs or vehicles 24 h post-transfection.

2.6. Degradation assay

COS7 cells were transiently transfected with wild-type or L347P PINK1-FLAG. Twenty-four hours after transfection, cells were treated with 100 μg/ml cycloheximide (CHX) to prevent protein synthesis, after which they were harvested in lysis buffer at the times indicated in Section 3. Protein concentrations were determined using a Coomassie Plus Protein Assay Reagent kit (Pierce), and equal amounts of protein were subjected to SDS-PAGE. The resolved proteins were transferred to PVDF membranes (Immobilon, Millipore) and analyzed by immunoblot analysis using anti-FLAG Ab, after which the bands were visualized using an enhanced chemiluminescence detection kit (Amersham Pharmacia).

3. Results

3.1. PINK1 forms a complex with both Hsp90 and Cdc37

To isolate PINK1-binding proteins, HEK293 cells were transiently transfected with C-terminal FLAG-tagged PINK1 (PINK1-FLAG), after which proteins in the cell lysates were immunoprecipitated using anti-FLAG M2 agarose, subjected to SDS-PAGE, and stained with CBB. As a control, the same purification procedure was undertaken with non-transfected HEK293 cells. We observed several bands in samples from PINK1-FLAG transfectants that were not discernable in the control sample (Fig. 1A). We then identified the proteins in those bands using standard tryptic peptide mass-spectrometric finger printing (Fig. 1B). Consistent with earlier results, two of the proteins were identified as PINK1, itself (Beilina et al., 2005; Silvestri et al., 2005; Petit et al., 2005; Park et al., 2006), while the others were identified as Hsp90, Hsp70 and Cdc37. Hsp90 and Cdc37 were previously reported to interact with a number of other protein kinases, including one encoded by the PD-related gene *LRRK2* (Gloeckner et al., 2006). We then confirmed the mass-spectral identification of PINK1-associated proteins by immunoblotting samples of the purified protein

Please cite this article in press as: Moriwaki, Y. et al., L347P PINK1 mutant that fails to bind to Hsp90/Cdc37 chaperones is rapidly degraded in a proteasome-dependent manner, Neurosci. Res. (2008), doi:10.1016/j.neures.2008.01.006

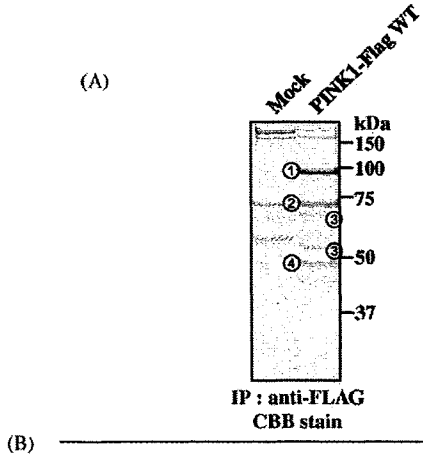

(B)

	Protein name	Score	% sequence converge
①	Hsp90	1623	56 %
②	Hsp70	720	34 %
③	PINK1	917	40 %
④	Cdc37	302	20 %

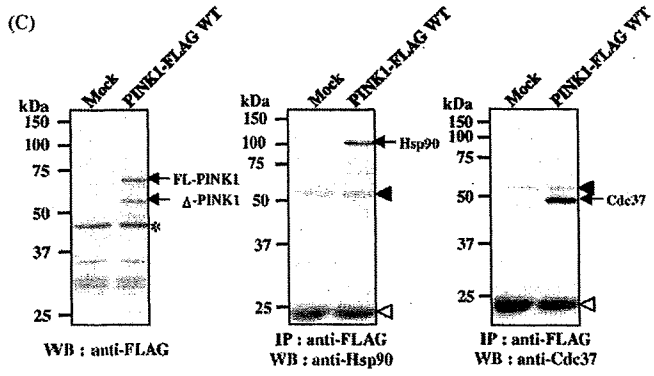

Fig. 1. PINK1 forms a complex with both Hsp90 and Cdc37. (A) HEK293 cells were transfected for 24 h with either a vector expressing PINK1-FLAG or with an empty vector (Mock). The transfectants were then lysed and immunoprecipitated with anti-FLAG Ab, the immunocomplexes were separated by SDS-PAGE, and the gel was stained with CBB to visualize proteins associated with PINK1. (B) CBB stained bands, labeled as indicated in (A), were excised from the gel and, following in-gel digestion with trypsin, their identities were determined by tryptic peptide mass-spectral fingerprinting. Scores and percentages of sequence converge for each protein identified are indicated. (C) The samples purified in (A) were immunoblotted with the indicated Abs; the asterisk indicates a non-specific band detected by anti-FALG Ab. Full length (FL) and processed PINK1 (Δ-PINK1) were detected. Closed and open arrowheads indicate IgG heavy and light chains, respectively.

with Abs against Hsp90, Cdc37 or FLAG (Fig. 1C). Taken together, these findings indicate that Hsp90 and Cdc37 specifically associate with PINK1.

3.2. *Hsp90 regulates PINK1 stability*

Hsp90 is a ubiquitous molecule that plays a key role in the stabilization and conformational regulation of various signaling effectors, including steroid hormone receptors and protein kinases (Young et al., 2001). To determine whether Hsp90 also regulates PINK1 stability, we next incubated COS7 cells transiently transfected with wild-type PINK1-FLAG with 1–10 μM GA, an inhibitor of Hsp90. We found that cells treated with 1 or 3 μM GA showed reduced levels of PINK1 (Fig. 2, top panel), whereas levels of Hsp90 and Cdc37 were unaffected (Fig. 2, middle and bottom panels). In addition, GA completely blocked the interaction between PINK1 and Hsp90/Cdc37. Examination of the time course of the response to GA revealed that levels of full-length PINK1 gradually declined by 90% over the course of 4 h after the addition of GA to COS7 cells (Fig. 3A). These findings were then confirmed using novobiocin, another known Hsp90 inhibitor that is structurally unrelated to GA and binds to the ATP-binding domain located in the C-terminal part of Hsp90 (Marcu et al., 2000). As shown in Fig. 3A, novobiocin treatment also significantly reduced levels of PINK1 in COS7 cells, and similar results were obtained with HEK293 cells (data not shown). The changes of PINK1 level induced by Hsp90 inhibitors are likely to be ascribable to its protein stability and degradation. First, PINK1 mRNA level was not affected by GA treatment as assessed by RT-PCR analysis (data not shown). Moreover, GA-induced PINK1 downregulation was suppressed by protease inhibitors (Fig. 3B).

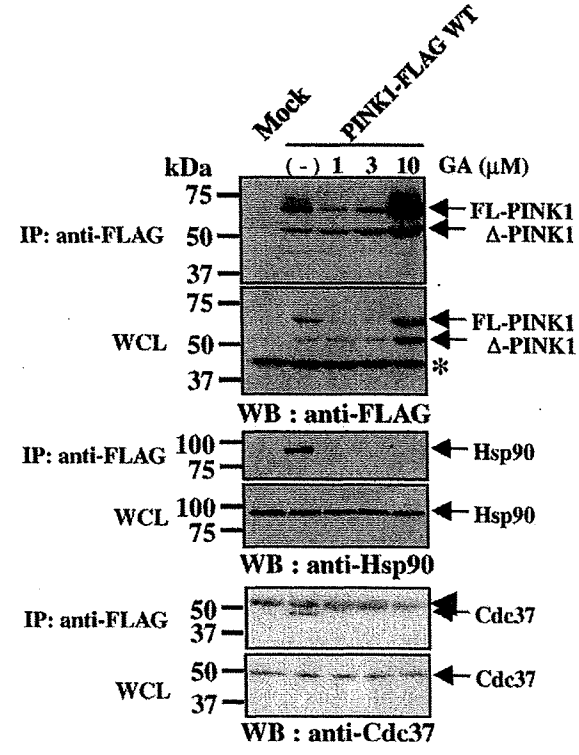

Fig. 2. GA treatment diminishes the interaction of PINK1 with both Hsp90 and Cdc37. COS7 cells were transfected for 24 h with either PINK1-FLAG or Mock expression vector and then treated with indicated concentration of GA. After incubating an additional 4 h, the cells were lysed and immunoprecipitated as described in Section 2. Immunocomplexes and whole-cell lysates (WCLs) were subjected to electrophoresis on polyacrylamide gel and immunoblotted with the indicated Abs; an asterisk indicates a non-specific band detected by anti-FALG Ab, which served as an internal control. The arrowhead indicates IgG heavy chain.

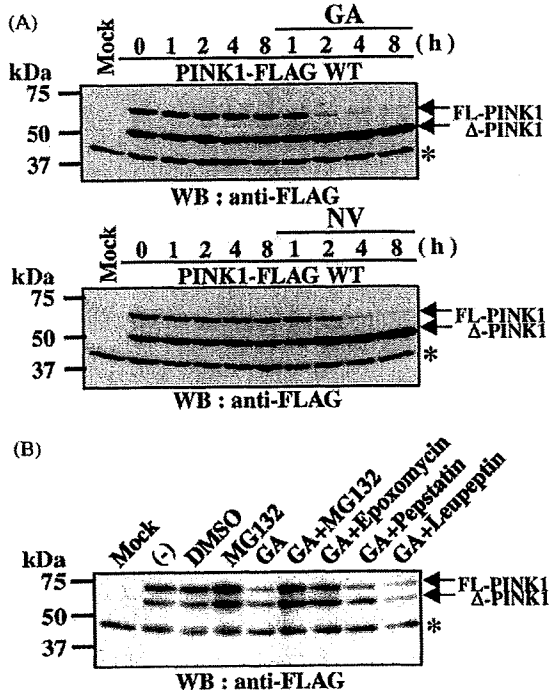

Fig. 3. PINK1 degradation is enhanced by Hsp90 inhibitors but inhibited by proteasome inhibitors. (A) COS7 cells were transiently transfected with PINK1-FLAG, after which the transfectants were incubated for the indicated times in the presence of 3 μM GA, 1 mM novobiocin (NV) or their vehicles (DMSO and water, respectively). After the indicated times or before the addition of drug (T0), the cells were lysed and their lysates were subjected to SDS-PAGE and immunoblotted with anti-FLAG M2 Ab. (B) COS7 cells transiently transfected with PINK1-FLAG were incubated for 4 h in the presence of GA or vehicle (DMSO). The proteasome inhibitors (epoxomycin or MG132) or lysosomal protease inhibitors (pepstatin or leupeptin) were simultaneously added in the presence or absence of GA. (−) indicates no drug treatment; the asterisk indicates a non-specific band detected by anti-FALG Ab, which served as an internal control.

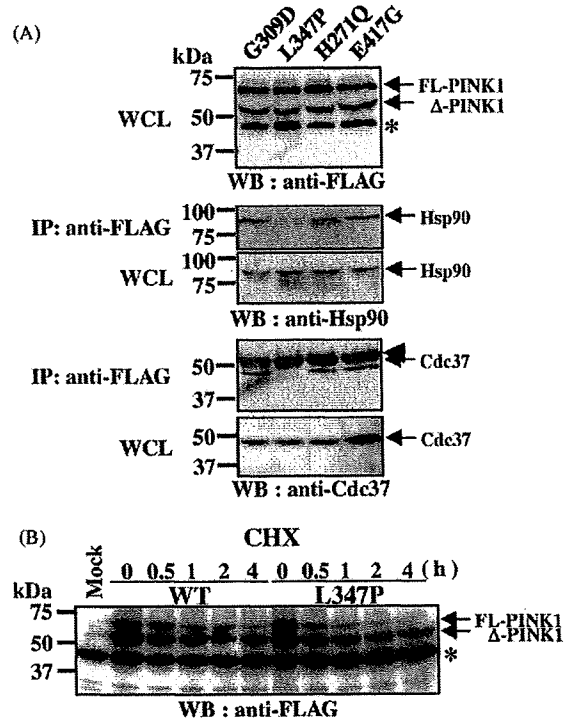

Fig. 4. Familial PD-associated L347P mutation impairs the interaction between PINK1 and Hsp90/Cdc37. (A) Wild-type PINK1 and PD-associated PINK1 mutants expressed in COS7 cells were immunoprecipitated with anti-FLAG Ab and immunoblotted with anti-Hsp90, anti-Cdc37 or anti-FLAG Ab. (B) COS7 cells were transfected for 24 h with either wild-type PINK1-FLAG or L347P mutant PINK1-FLAG, after which they were incubated for the indicated times in the presence of 100 μg/ml cycloheximide (CHX). After the indicated times or before the addition of CHX, cells were resuspended in lysis buffer, and the proteins were analyzed by immunoblotting using anti-FLAG M2 Ab. Similar results were obtained in two independent experiments. The asterisk indicates a non-specific band detected by anti-FALG Ab, which served as an internal control. The arrowhead indicates IgG heavy chain.

Several studies have shown that GA-induced degradation of Hsp90 target proteins is preceded by their ubiquitination and subsequent targeting by proteasome (Miyata et al., 2001; Nony et al., 2003; Boudeau et al., 2003; An et al., 2000). To determine whether GA-mediated decay of PINK1 is also dependent on proteasomal degradation, we blocked proteasome function using two specific inhibitors, epoxomycin and MG132. We found that when COS7 cells expressing PINK1-FLAG were incubated with GA plus either epoxomycin or MG132, but not with other protease inhibitors, degradation of full-length PINK1 was prevented (Fig. 3B). Apparently, upon dissociation of the PINK1–Hsp90 complex, PINK1 is degraded by proteasome.

3.3. Familial PD-associated L347P mutation impairs the interaction between PINK1 and Hsp90/Cdc37

Beilina et al. (2005) recently reported the L347P PINK1 mutant is much more rapidly degraded within cells than wild-type PINK1. To clarify the molecular mechanism underlying the enhanced degradation of the PINK1 mutant, we tested whether PINK1 missense mutants found in familial PD patients (Valente et al., 2004; Hatano et al., 2004) show diminished binding to Hsp90 and/or Cdc37/p50. Immunoprecipitation of PINK1 mutants using anti-FLAG Ab followed by immunoblotting with anti-Hsp90 or Cdc37/p50 Ab revealed that the L347P substitution mutant did not bind to either Hsp90 or Cdc37/p50, whereas the other PD-linked mutations we tested here did not significantly affect the interaction of PINK1 with Hsp90/Cdc37 (Fig. 4A). To confirm the effect of the L347P mutation on protein stability, we also carried out a protein degradation assay and found that the half-life of full-length wild-type PINK1 was 1 h, whereas the half-life of the full-length L347P PINK1 mutant was only 30 min (Fig. 4B). Thus the inability to bind to Hsp90 appears to substantially reduce the stability of the L347P PINK1 mutant.

4. Discussion

Our findings indicate that the molecular chaperone complex Hsp90/Cdc37 bind to PINK1 and thus regulate its stability. Hsp90 is an abundant cytoplasmic protein that functions as a

Please cite this article in press as: Moriwaki, Y., et al., L347P PINK1 mutant that fails to bind to Hsp90/Cdc37 chaperones is rapidly degraded in a proteasome-dependent manner, Neurosci. Res. (2008), doi:10.1016/j.neures.2008.01.006

chaperone and plays an essential role in numerous cellular processes. With fewer target proteins than Hsp60 or Hsp70, Hsp90 appears to primarily bind protein kinases and hormone receptors (Young et al., 2001). To specifically interact with its client proteins, Hsp90 also requires the presence of co-chaperones. One of these, Cdc37/p50, appears to specifically target Hsp90 to a variety of protein kinases, including the mitogen-activated protein kinase (MAPK) family member MAPK-overlapping kinase (MOK) (Miyata et al., 2001), LBK1 (Nony et al., 2003; Boudeau et al., 2003), IKK (Chen et al., 2002) and LRRK2 (Gloeckner et al., 2006). One of the Hsp90/Cdc37 binding proteins IKK was reported to independently bind to both Cdc37 and Hsp90. However, treatment with Hsp90 inhibitors such as GA abolishes the binding ability of IKK to bind both Hsp90 and Cdc37, leading to disruption of its activity. These findings, along with several lines of evidence by the other researchers, suggest that Hsp90 functions in concert with Cdc37 and their interaction is important in their stabilization, activation and/or translocation. Although there is a possibility that Hsp90 and Cdc37 independently bind to PINK1, treatment with Hsp90 inhibitors markedly reduced levels of PINK1 indicate Hsp90/Cdc37 complex are key regulator for PINK1 stability.

Hsp90/Cdc37 interacts with the catalytic domains of several kinases, thereby affecting their enzymatic activity. For example, the interaction of the IKK complex with Hsp90/Cdc37 is required for its activation by tumor necrosis factor (Chen et al., 2002), and the interaction of CDK4 with Hsp90/Cdc37 is required for its proper assembly with cyclin D (Dai et al., 1996). By contrast, the kinase activity of the LKB1 is unaffected by its binding to Hsp90/Cdc37 (Nony et al., 2003). Some recent studies have shown that recombinant PINK1 expressed in *Escherichia coli* has kinase activity (Silvestri et al., 2005; Hatano et al., 2004), but it is not clear whether PINK1 expressed in mammalian cells has similar activity. In our hands, PINK1 exhibited no self-directed phosphorylation activity (data not shown). Further investigation will be required to clarify this issue.

Another function of Hsp90 is stabilization of its target proteins through the prevention of their degradation by the proteasome system. A number of oncogenes, including v-Src (An et al., 2000) and MOK (Miyata et al., 2001), are rapidly degraded in cells following treatment with GA. Consistent with the idea that Hsp90 is a key regulator of PINK1 stability, treatment with Hsp90 inhibitors markedly reduced PINK1 levels within cells (Figs. 2 and 3), while two proteasome inhibitors, epoxomycin and MG132, each prevented Hsp90-inhibitor-induced PINK1 degradation (Fig. 3).

In the present study, we found high concentration of GA treatment conversely augmented PINK1 protein level. Hsp90 was known to form complex with heat shock transcription factor Hsf1, and when this interaction was impaired by adding Hsp90 inhibitor, Hsf1 can form active trimers which enhance the transcription of a subset of genes. According to this idea, other factor(s) induced by Hsf1 may also influence on PINK1 stability.

Beilina et al. (2005) showed that when expressed in either *E. coli* or mammalian cells, steady-state level of the L347P PINK1 mutant is low. They suggested this was the result of enhanced degradation caused by disruption of α-helix similar to that observed in the L166P DJ-1 mutant (Miller et al., 2003). However, we did not observe low steady-state level of L347P PINK1 mutant protein expressed in *E. coli* (data not shown). Instead, the present results suggest that the diminished stability of the L347P PINK1 mutant reflects its inability to interact with Hsp90/Cdc37.

PINK1 reportedly reduces basal neuronal pro-apoptotic activity and protects neurons from staurosporine-induced apoptosis (Silvestri et al., 2005). In addition, Deng et al. (2005) showed that treating cells with PINK1-specific siRNA reduced their viability and significantly increased the cytotoxicity of MPP^+ and rotenone. We found that the L347P mutation diminishes both the interaction of PINK1 with Hsp90 and its stability. These results indicate that L347P mutant PINK1 loses its cell protective function due to destabilization, resulting in the development of PD. Moreover, the present results suggest possible contribution of chaperon system, especially Hsp90, to the pathogenesis of PARK6.

During the preparation of this manuscript, Weihofen et al. (2007) reported that PINK1 interact with Hsp90/Cdc37 complex. They showed GA treatment that affects Hsp90 and client protein interaction preferentially reduced the level of endogenous full-length PINK1. Our findings are consistent with their observations (Figs. 2 and 3). In the present study, we, for the first time, showed that L347P mutant PINK1 displayed diminished interaction with Hsp90/Cdc37, resulting in its instability. Again, these results indicate that L347P mutant PINK1 loses its cell protective function due to destabilization, leading to the development of PD.

Acknowledgements

We thank Dr. Yasuyuki Suzuki for his critical advice and helpful discussions. This study was supported in part by research grants from RIKEN BSI, and a grant-in-aid from the Ministry of Education, Culture, Sports, and Technology of Japan.

References

Abou-Sleiman, P.M., Muqit, M.M., Wood, N.W., 2006. Expanding insights of mitochondrial dysfunction in Parkinson's disease. Nat. Rev. Neurosci. 7, 207–219 review.

An, W.G., Schulte, T.W., Neckers, L.M., 2000. The heat shock protein 90 antagonist geldanamycin alters chaperone association with p210bcr-abl and v-src proteins before their degradation by the proteasome. Cell Growth Differ. 11, 355–360.

Beilina, A., Van Der Brug, M., Ahmad, R., Kesavapany, S., Miller, D.W., Petsko, G.A., Cookson, M.R., 2005. Mutations in PTEN-induced putative kinase 1 associated with recessive parkinsonism have differential effects on protein stability. Proc. Natl. Acad. Sci. U.S.A. 102, 5703–5708.

Boudeau, J., Deak, M., Lawlor, M.A., Morrice, N.A., Alessi, D.R., 2003. Heat-shock protein 90 and Cdc37 interact with LKB1 and regulate its stability. Biochem. J. 370, 849–857.

Chen, G., Cao, P., Goeddel, D.V., 2002. TNF-induced recruitment and activation of the IKK complex require Cdc37 and Hsp90. Mol. Cell 9, 401–410.

Clark, I.E., Dodson, M.W., Jiang, C., Cao, J.H., Huh, J.R., Seol, J.H., Yoo, S.J., Hay, B.A., Guo, M., 2006. Drosophila pink1 is required for mitochondrial function and interacts genetically with parkin. Nature 441, 1162–1166.

Dai, K., Kobayashi, R., Beach, D., 1996. Physical interaction of mammalian CDC37 with CDK4. J. Biol. Chem. 271, 22030–22034.

Dauer, W., Przedborski, S., 2003. Parkinson's disease: mechanisms and models. Neuron 39, 889–909 review.

Deng, H., Jankovic, J., Guo, Y., Xie, W., Le, W., 2005. Small interfering RNA targeting the PINK1 induces apoptosis in dopaminergic cells SH-SY5Y. Biochem. Biophys. Res. Commun. 337, 1133–1138.

Gloeckner, C.J., Kinkl, N., Schumacher, A., Braun, R.J., O'Neill, E., Meitinger, T., Kolch, W., Prokisch, H., Ueffing, M., 2006. The Parkinson disease causing LRRK2 mutation I2020T is associated with increased kinase activity. Hum. Mol. Genet. 15, 223–232.

Hatano, Y., Li, Y., Sato, K., Asakawa, S., Yamamura, Y., Tomiyama, H., Yoshino, H., Asahina, M., Kobayashi, S., Hassin-Baer, S., Lu, C.S., Ng, A.R., Rosales, R.L., Shimizu, N., Toda, T., Mizuno, Y., Hattori, N., 2004. Novel PINK1 mutations in early-onset parkinsonism. Ann. Neurol. 56, 424–427.

Marcu, M.G., Chadli, A., Bouhouche, I., Catelli, M., Neckers, L.M., 2000. The heat shock protein 90 antagonist novobiocin interacts with a previously unrecognized ATP-binding domain in the carboxyl terminus of the chaperone. J. Biol. Chem. 275, 37181–37186.

Miller, D.W., Ahmad, R., Hague, S., Baptista, M.J., Canet-Aviles, R., McLendon, C., Carter, D.M., Zhu, P.P., Stadler, J., Chandran, J., Klinefelter, G.R., Blackstone, C., Cookson, M.R., 2003. L166P mutant DJ-1, causative for recessive Parkinson's disease, is degraded through the ubiquitin-proteasome system. J. Biol. Chem. 278, 36588–36595.

Mineki, R., Taka, H., Fujimura, T., Kikkawa, M., Shindo, N., Murayama, K., 2002. In situ alkylation with acrylamide for identification of cysteinyl residues in proteins during one- and two-dimensional sodium dodecyl sulphate-polyacrylamide gel electrophoresis. Proteomics 2, 1672–1681.

Miyata, Y., Ikawa, Y., Shibuya, M., Nishida, E., 2001. Specific association of a set of molecular chaperones including HSP90 and Cdc37 with MOK, a member of the mitogen-activated protein kinase superfamily. J. Biol. Chem. 276, 21841–21848.

Nakajima, A., Kataoka, K., Hong, M., Sakaguchi, M., Huh, N.H., 2003. BRPK, a novel protein kinase showing increased expression in mouse cancer cell lines with higher metastatic potential. Cancer Lett. 201, 195–201.

Nony, P., Gaude, H., Rossel, M., Fournier, L., Rouault, J.P., Billaud, M., 2003. Stability of the Peutz-Jeghers syndrome kinase LKB1 requires its binding to the molecular chaperones Hsp90/Cdc37. Oncogene 22, 9165–9175.

Park, J., Lee, S.B., Lee, S., Kim, Y., Song, S., Kim, S., Bae, E., Kim, J., Shong, M., Kim, J.M., Chung, J., 2006. Mitochondrial dysfunction in Drosophila PINK1 mutants is complemented by parkin. Nature 441, 1157–1161.

Petit, A., Kawarai, T., Paitel, E., Sanjo, N., Maj, M., Scheid, M., Chen, F., Gu, Y., Hasegawa, H., Salehi-Rad, S., Wang, L., Rogaeva, E., Fraser, P., Robinson, B., St. George-Hyslop, P., Tandon, A., 2005. Wild-type PINK1 prevents basal and induced neuronal apoptosis, a protective effect abrogated by Parkinson disease-related mutations. J. Biol. Chem. 280, 34025–34032.

Silvestri, L., Caputo, V., Bellacchio, E., Atorino, L., Dallapiccola, B., Valente, E.M., Casari, G., 2005. Mitochondrial import and enzymatic activity of PINK1 mutants associated to recessive parkinsonism. Hum. Mol. Genet. 14, 3477–3492.

Unoki, M., Nakamura, Y., 2001. Growth-suppressive effects of BPOZ and EGR2, two genes involved in the PTEN signaling pathway. Oncogene 20, 4457–4465.

Tang, B., Xiong, H., Sun, P., Zhang, Y., Wang, D., Hu, Z., Zhu, Z., Ma, H., Pan, Q., Xia, J.H., Xia, K., Zhang, Z., 2006. Association of PINK1 and DJ-1 confers digenic inheritance of early-onset Parkinson's disease. Hum. Mol. Genet. 15, 1816–1825.

Valente, E.M., Abou-Sleiman, P.M., Caputo, V., Muqit, M.M., Harvey, K., Gispert, S., Ali, Z., Del Turco, D., Bentivoglio, A.R., Healy, D.G., Albanese, A., Nussbaum, R., Gonzalez-Maldonado, R., Deller, T., Salvi, S., Cortelli, P., Gilks, W.P., Latchman, D.S., Harvey, R.J., Dallapiccola, B., Auburger, G., Wood, N.W., 2004. Hereditary early-onset Parkinson's disease caused by mutations in PINK1. Science 304, 1158–1160.

Weihofen, A., Ostaszewski, B., Minami, Y., Selkoe, D.J., 2007. Pink1 Parkinson mutations, the Cdc37/Hsp90 chaperones and Parkin all influence the maturation or subcellular distribution of Pink1. Hum. Mol. Genet. (Epub ahead of print).

Young, J.C., Moarefi, I., Hartl, F.U., 2001. Hsp90: a specialized but essential protein-folding tool. J. Cell Biol. 154, 267–273.

Please cite this article in press as: Moriwaki, Y., et al., L347P PINK1 mutant that fails to bind to Hsp90/Cdc37 chaperones is rapidly degraded in a proteasome dependent manner, Neurosci. Res. (2008), doi:10.1016/j.neures.2008.01.006

BRIEF COMMUNICATIONS

nature neuroscience

Astrocytes as determinants of disease progression in inherited amyotrophic lateral sclerosis

Koji Yamanaka[1,2], Seung Joo Chun[1], Severine Boillee[1], Noriko Fujimori-Tonou[2], Hirofumi Yamashita[2], David H Gutmann[3], Ryosuke Takahashi[4], Hidemi Misawa[5] & Don W Cleveland[1]

Dominant mutations in superoxide dismutase cause amyotrophic lateral sclerosis (ALS), an adult-onset neurodegenerative disease that is characterized by the loss of motor neurons. Using mice carrying a deletable mutant gene, diminished mutant expression in astrocytes did not affect onset, but delayed microglial activation and sharply slowed later disease progression. These findings demonstrate that mutant astrocytes are viable targets for therapies for slowing the progression of non–cell autonomous killing of motor neurons in ALS.

ALS is an adult-onset neurodegenerative disease, characterized by a progressive and fatal loss of motor neurons. Dominant mutations in the gene for superoxide dismutase (*SOD1*) are the most frequent cause of inherited ALS. Ubiquitous expression of mutant *SOD1* in rodents leads to progressive, selective motor neuron degeneration as a result of acquired toxic properties. The exact mechanism responsible for motor neuron degeneration in ALS, however, is not known[1,2]. Mutant damage in the vulnerable motor neurons is a key determinant of disease onset[3], whereas accumulating evidence supports an active role of non-neuronal cells in motor neuron degeneration[3–7]. Evidence with selective gene excision[3] or bone-marrow grafting[5] has demonstrated that mutant SOD1-derived damage in microglia accelerates later disease progression. Despite the importance of astrocyte function, the role of mutant action in astrocytes in disease has not been tested *in vivo*.

To examine whether mutant SOD1 damage in astrocytes contributes to disease, *loxSOD1*^{G37R} mice[3], carrying a mutant *SOD1* gene that can be deleted by the action of the Cre recombinase, were mated with *GFAP-Cre* mice (**Fig. 1** and **Supplementary Fig. 1** online), which express both Cre recombinase and β-galactosidase (*LacZ*) under the control of the human GFAP promoter[8]. Mice from these matings that carry the *GFAP-Cre* transgene are denoted as Cre$^+$, whereas mice without it are referred to as Cre$^-$. To determine the cell-type specificity of Cre expression in the spinal cord, *GFAP-Cre* mice were mated to Rosa26 mice, which ubiquitously express a *LacZ* gene that encodes functional β-galactosidase only after Cre-mediated recombination. Although this *GFAP-Cre* transgene is expressed in a subset of neurons in the cerebellum and hippocampus during embryogenesis[9], measurement of β-galactosidase activity (by deposition of a blue reaction product after addition of the X-gal substrate) demonstrated that Cre expression and Cre-mediated recombination was restricted in the spinal cord to GFAP-reactive astrocytes (**Fig. 1a,b**). The efficiency of mutant gene excision in cultured astrocytes from newborn *loxSOD1*^{G37R}*/GFAP-Cre*$^+$ mice was ~76% (**Fig. 1d,e**), determined by quantitative PCR for human SOD1 transgene number (**Fig. 1d**) and immunoblotting for mutant SOD1 levels (**Fig. 1e**). We observed neither detectable Cre activity nor mutant gene excision in microglia (**Fig. 1c** and **Supplementary Fig. 2** online).

A simple, objective measure of disease onset and early disease was applied by initiation of weight loss, itself reflecting denervation-induced muscle atrophy. Reduction of SOD1^{G37R} in astrocytes did not slow disease onset nor early disease (GFAP-Cre$^+$, 341.6 ± 48.9 d; GFAP-Cre$^-$, 337.0 ± 35.8 d; **Fig. 1f,h**). However, late disease progression (from early disease to end stage) was sharply delayed, providing a mean extension of survival by 48 d (Cre$^+$, 87.4 d; Cre$^-$, 39.5 d; **Fig. 1j**). Progression from onset to early disease was more modestly slowed by 14 d (Cre$^+$, 99.3 d; Cre$^-$, 85.2 d; **Fig. 1i**). Overall survival was extended by 60 d (Cre$^+$, 436.5 ± 38.8 d; Cre$^-$, 376.5 ± 26.9 d; **Fig. 1g**). This contrasts with delayed disease onset from diminished mutant synthesis solely within motor neurons (with a *VAChT-Cre* transgene carrying the motor neuron–specific vesicular acetylcholine transporter promoter) without affecting disease progression (**Supplementary Results**, **Supplementary Methods** and **Supplementary Fig. 3** online), just as reported previously with an *Isl1* (*Islet1*)*-Cre* transgene that is expressed in motor neurons and some peripheral tissues[3].

Astrocytic and microglial cell activation is a well-accepted feature of SOD1 mutant–mediated ALS[1,2]. An elevated proportion of GFAP-positive astrocytes appeared before disease onset (**Fig. 2a**) in *loxSOD1*^{G37R} mice. This astrogliosis was progressive, readily apparent by onset (**Fig. 2b**) and more prominent during disease progression (**Fig. 2c**). Despite substantial mutant reduction, astrogliosis was not, however, different in comparing disease-matched *loxSOD1*^{G37R}*/GFAP-Cre*$^+$ mice (**Fig. 2d,e**) and *loxSOD1*^{G37R}*/GFAP-Cre*$^-$ mice (**Fig. 2b,c**).

Microglial activation occurred at earliest disease onset in *Cre*$^-$ mice (**Fig. 2g**) and was progressively more prominent during disease progression (**Fig. 2h**). Microglial activation was, however, substantially delayed from onset through early disease in the *GFAP-Cre*$^+$ mice when mutant SOD1 levels were reduced only in astrocytes (**Fig. 2i,j**). By exploiting the presence of β-galactosidase to mark astrocytes with diminished SOD1 mutant synthesis, examination of sections throughout lumbar spinal cords of symptomatic *loxSOD1*^{G37R}*/GFAP-Cre*$^+$ mice

[1]Ludwig Institute for Cancer Research and Department of Medicine and Neuroscience, University of California at San Diego, 9500 Gilman Drive, La Jolla, California 92093-0670, USA. [2]Yamanaka Research Unit, RIKEN Brain Science Institute, 2-1 Hirosawa, Wako, Saitama 351-0198, Japan. [3]Department of Neurology, Washington University School of Medicine, 660 South Euclid Avenue, St. Louis, Missouri 63110, USA. [4]Department of Neurology, Graduate School of Medicine, Kyoto University, 54 Shogoin Kawahara-cho, Sakyo-ku, Kyoto 606-8507, Japan. [5]Department of Pharmacology, Kyoritsu University of Pharmacy, 1-5-30 Shibakoen, Minato-ku, Tokyo 105-8512, Japan. Correspondence should be addressed to D.W.C. (dcleveland@ucsd.edu) or K.Y. (kyamanaka@brain.riken.jp).

Received 26 November 2007; accepted 7 January 2008; published online 3 February 2008; doi:10.1038/nn2047